# WAKE BEHAVIOR DOWNSTREAM OF A TRANSONIC COMPRESSOR ROTOR

by

Harry E. Stephens III

GTL Report No. 118 August 1974

GAS TURBINE LABORATORY
MASSACHUSETTS INSTITUTE OF TECHNOLOGY
CAMBRIDGE, MASSACHUSETTS

# WAKE BEHAVIOR DOWNSTREAM OF A TRANSONIC COMPRESSOR ROTOR

by

Harry E. Stephens III

GTL Report No. 118 August 1974

## ABSTRACT

Measurements of the static pressure resolved in radial and axial directions downstream of a transonic compressor rotor have been harmonically analyzed. The investigation is part of a program addressing the behavior of disturbances in strongly swirling flows. There is evidence that the wakes are radially outward and carry static pressure disturbances with them. The harmonic analysis of the static pressure measured at the tip radius indicates a shift toward higher frequency of the peak in the power spectrum as the flow proceeds downstream. It is suggested that this increasing frequency associated with the power peak results from the wakes being convected downstream in a fluid which has increasing swirl velocity as it travels away from the rotor.

## ACKNOWLEDGEMENTS

The author would like to express his sincere appreciation to all of the members of the Gas Turbine Laboratory who contributed to this work. Foremost among these is Professor J. L. Kerrebrock, whose guidance and suggestions were instrumental in all phases of this research. Messrs. A. H. Epstein and W. T. Thompkins offered much of their time assisting in the experimental work and also provided many helpful suggestions during frequent discussions.

The research was performed on the Blowdown Compressor, constructed under NASA Grant NGL-22-009-383, while support in the form of a Research Assistantship was provided the author by Pratt & Whitney Aircraft, Division of United Aircraft Corporation.

TABLE OF CONTENTS

# CHAPTER I

## INTRODUCTION

The fundamental objective of the turbomachinery designer is to devise a machine which transfers energy to or from the working fluid in the most efficient manner possible. A thorough understanding of the working fluid as it moves through the machine would enable the engineer to optimize his design configuration. At present, no theories are available to completely describe the complex, three-dimensional flow pattern which exists within the blade rows of modern high work, high Mach number axial flow compressors.

Contemporary compressor designs are based largely on semi-empirical methods which make extensive use of data taken from cascades of stationary airfoils. Empirical correction factors have been devised to compensate for the reduced annulus area resulting from the developing boundary layers on the hub and outer casing. Similarly, analysis of cascade data provides information on the deviation of the fluid exit angle from the blade exit angle. Other empirical correlations determine the limits of the diffusion process and are vital in avoiding excessive separation of the flow from the blade surfaces. This information is used to design blading profiles at individual radii or along individual streamlines. It is important to note that the flow in cascades of stationary airfoils does not include the effects of centrifugal forces and the resulting radial flows which arise from the rotor rotation in high speed compressors.

Recently, Evans [1] measured the free stream turbulence level and the unsteadiness due to periodic fluctuations in both the mean velocity

and the air angle at the inlet to a compressor stator row. Two single stage experimental compressors were used in his investigation. Both have 6 in. chord C-4 rotor blading of 18 in. span which is designed for free vortex velocity distribution. One compressor consists of a single 22-blade rotor row, while the second has a 24-blade rotor followed by a 15-blade stator. Both rigs are low speed compressors operating at 650 rpm which results in a tip speed of 170 ft./sec.

In this paper, the flow field downstream of a full scale transonic compressor rotor representative of modern high speed designs is investigated. The two-foot diameter transonic rotor is designed for a tangential Mach number of 1.2 and a nominal pressure ratio of 1.6. Here, the effects of compressibility and three-dimensional flow complicate attempts to theoretically predict the resulting flow field. Haines [2] has made radial and axial measurements of the wake structure behind this rotor to give preliminary estimates of the wake positioning, spreading and decay rates in the downstream flow.

Noise and losses associated with the periodic unsteadiness in the pressure field might be reduced to a considerable extent if the primary sources of these disturbances, as well as their behavior in the rotor exit flow could be identified. It is expected that the blade wakes should play an important role in determining the pressure field in the rotor blade passages, in addition to being an important source of noise in turbomachines. This study represents an attempt to describe the nature and behavior of these pressure disturbances. A harmonic analysis of the downstream pressure map should give some insight into what part of the disturbance

is attributable to the wake. In addition, this type of data reduction should indicate whether or not other periodic disturbances or harmonics of blade passing frequency are important.

# CHAPTER II

## THE BLOWDOWN FACILITY

The MIT Compressor Blowdown Facility is designed to permit detailed aerodynamic studies of the flow through a full scale transonic compressor rotor. Kerrebrock [3, 4] gives a detailed description of the facility, including the design procedure and a summary of the aerodynamic data obtained from the blowdown tests.

The blowdown facility consists of three sections: a supply tank, the rotor test section, and a dump tank. See Figure 1. A pre-formed soft grade aluminum diaphragm initially separates the supply tank from the test section. Prior to a run, the entire facility is pumped down to vacuum with the diaphragm in place. Next, the supply tank is filled with a mixture of argon and freon, having a ratio of specific heats of 1.4 and a speed of sound of 840 ft./sec. This low sound speed enables high rotor tip Mach numbers with less severe centrifugal stresses. After the supply tank is filled with the gas mixture, the rotor is brought to speed in vacuum by an electric motor mounted within the test section. When the design speed of 10,000 rpm is reached, a blasting cap is triggered which, in turn, detonates strips of explosive material attached in a star shaped pattern to the rotor facing side of the diaphragm. The diaphragm is segmented into eight petals which are forced open by the pressure of the gas in the supply tank. The diaphragm takes approximately 10 msec. to open fully. The test gas expands through the test section and into the dump tank. During this time, the rotor is driven by its own inertia. The facility was sized so that the decrease in supply tank total temperature is matched with the

rotor deceleration in such a manner that a steady flow test condition exists for some 40 msec. During the test, static pressure measurements are made in the test section outer casing at axial locations both upstream and downstream of the rotor. Figure 2 shows the location of each of the instrumentation ports which are spaced at intervals of one axial chord. In addition, two traversing probes are fired radially into the test section to give radial profiles of total and static pressure. One of the traversing probes measures circumferential and radial flow angles as well. The pressure transducers employed for both the traversing probes and for the wall static measurements are Kulite Corp. miniature silicon bonded strain gauge transducers. The diaphragms are approximately 0.080 in. in diameter and have a frequency response flat to about 100 kHz, when used in the wall static application. These same transducers give a frequency response flat to about 50 kHz, when mounted in the specially developed traversing probes. In both applications, the Kulite gauges have sufficient frequency response to give detailed measurements of pressure fluctuations many times the blade passing frequency (about 4 kHz).

All of the aerodynamic measurements made during the blowdown test are recorded on a fourteen channel FM instrumentation tape recorder running at a speed of 120 in. per sec. When detailed analysis of the data sample is desired, the tape recorder can be played back at speeds as low as 1 7/8 in. per sec. to give a 64-fold expansion of the time scale. This output can be displayed on an oscilloscope, recorded on strip charts, or transmitted to an analog to digital converter designed to interface with the MIT Information Processing Center.

# CHAPTER III

## DETAILS OF THE EXPERIMENT

As stated previously, this study represents an attempt to describe the nature and behavior of the static pressure fluctuations downstream of a transonic compressor rotor. In order to accomplish this, a map of the static pressure measured at various axial and radial locations was desired. One of the forementioned traversing probes consists of two Kulite diaphragms mounted as shown in Figure 3. One part is a conventional total pressure probe. The other measures static pressure, within a few percent of the dynamic pressure, by utilizing the cancelling effects of several pressure taps arranged around a cylinder, and feeding the cavity monitored by the transducer. To construct a pressure map of the downstream flow field, the traversing probe was first mounted in the instrumentation port directly behind the rotor (Port 5). During the test, the traverser was fired to the mean radius of the rotor blading and halted there to measure static pressure as a function of time. The probe was then remounted in Port 6 and Port 7 on successive tests and again fired to the mean radius. This procedure gives an axial survey of static pressure for a given radial position. The same procedure was repeated for radial locations at the tip of the rotor blading, as well as at the hub. For the hub and tip radial surveys, the probe was positioned at a radial location 1/2 in. from the rotor hub fairing, and 1/2 in. from the tip boundary layer bleed, respectively. This was done to avoid the major portion of the boundary layers growing on the inner and outer annuli.

The output voltage from the Kulite transducers is dependent upon the excitation voltage, in this case about 5.5 volts. A typical output

voltage is on the order of 40 millivolts. This voltage is then amplified to about 1.0 volts to be suitable for the input stage of the tape recorder. Two types of amplifiers are used for this purpose. The first gives a d.c. level in addition to the a.c. component. The second has excellent frequency response but no d.c. level. Since the information of interest in this study is the fluctuating component, the a.c.-only amplifier was selected. This decision imposes one restriction on the data analysis; relative rather than absolute values of pressure are on record.

During the steady flow portion of the test, the rotor decelerates roughly 5.5% of its initial speed. An harmonic analysis would then indicate a shifting frequency for blade passing over the period of the test. To avoid this problem, the tachometer signal, which is generated by a magnetic pick-up mounted on the rotor shaft, is used as an input to the spectrum analyzer's external sampling rate. In this way, the ratio of frequency to shaft rotational frequency remains fixed throughout the harmonic analysis. The output of the spectrum analyzer is then power as a function of frequency ratio (m) rather than pure frequency. In this case, blade passing frequency is fixed at 23 since the rotor contains 23 blades.

The analyzer continuously updates a memory of fixed length which is harmonically analyzed. In order to analyze a particular segment of the blowdown test time, it is necessary to trigger the analyzer to a memory hold condition at the end of the desired data segment. The following simplified block diagram illustrates how this is accomplished.

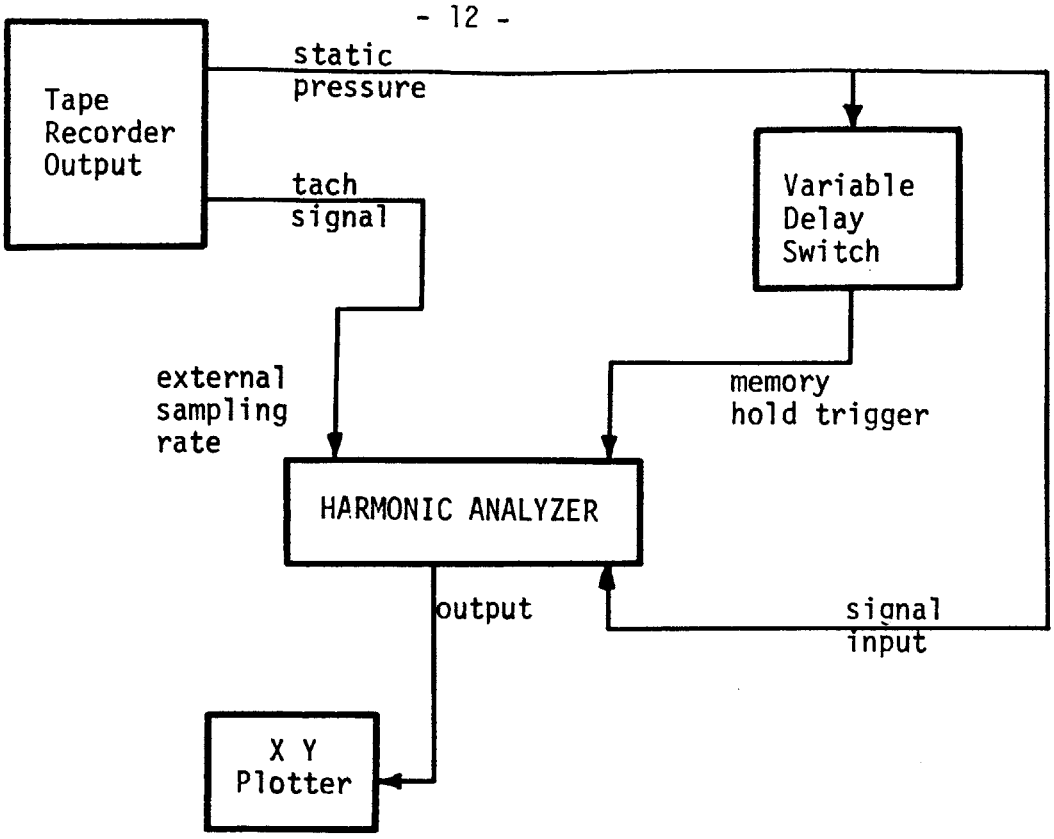
Tape
Recorder
Output
static
pressure
tach
signal
Variable
Delay
Switch
external
sampling
rate
memory
hold trigger
HARMONIC ANALYZER
output
signal
input
X Y
Plotter

# CHAPTER IV

# RESULTS

## 4.1 Experimental Results

The static pressure at each axial and radial location was harmonically analyzed with a Federal Scientific Ubiquitous Spectrum Analyzer (Model UA-14). Table 1 contains a listing of each harmonic analysis performed. Of the various time samples harmonically analyzed, those with the 100 msec. memory hold delay provided the most information.

The length of the analyzer's memory is determined by the sampling rate, which, in this case, is generated by the rotor tachometer signal. The resulting 60 msec. data sample extends from 40 to 100 msec. of test time, although steady flow conditions are not attained until some 80 msec. into the run. Repeating the harmonic analysis of a particular pressure record with delays ranging from 80 to 110 msec. shows very little change in the qualitative information contained in the results. This is offered in support of the contention that the use of some non-steady flow data has little effect on the results of the harmonic analysis.

In all of the harmonic analysis figures, the abscissa is labeled frequency ratio; that is, the ratio of frequency to shaft rotational frequency. The ordinate is a logarithmic scale of the amplitude in decibels. This is merely a means of judging the relative amplitudes between individual frequency ratios. It actually represents the ratio of the static pressure transducer output voltage to the internally generated reference voltage of the analyzer. The absolute magnitude of the maximum pressure fluctuations, determined by measuring them as recorded on an oscillograph

TABLE 1

SUMMARY OF HARMONIC ANALYSES

| Harmonic Analysis Date | Run Number | Transducer | Radial Location | Port | Memory Hold Delay (msec.) 80 | 90 | 100 | 110 | 130 |
|---|---|---|---|---|---|---|---|---|---|
| 03 May 74 | 99 | Probe | Mean | 5 | x | x | x | x | x |
| 11 July | 99 | Probe | Mean | 5 | | | x | | |
| 03 May | 97 | Probe | Mean | 6 | | x | x | x | |
| 03 May | 98 | Probe | Mean | 7 | | | x | x | |
| 03 May | 100 | Probe | Tip | 5 | | x | x | x | |
| 14 July | 100 | Probe | Tip | 5 | | | x | | |
| 03 May | 101 | Probe | Tip | 6 | | | x | x | |
| 13 July | 104 | Probe | Tip | 7 | | x | x | x | |
| 03 May | 103 | Probe | Tip | 7 | | | x | x | |
| 13 July | 103 | Probe | Tip | 7 | | | x | | |
| 03 May | 102 | Probe | Hub | 5 | | | x | x | |
| 12 July | 102 | Probe | Hub | 5 | | x | x | x | |
| 12 July | 113 | Probe | Hub | 6 | | x | x | x | |
| 11 July | 109 | Probe | Hub | 7 | | x | x | x | |
| 14 July | 109 | Probe | Hub | 7 | | x | x | x | |
| 12 July | 113 | Wall | | 5 | | x | x | x | |
| 12 July | 109 | Wall | | 5 | | x | x | x | |
| 03 May | 98 | Wall | | 5 | | | x | x | |
| 03 May | 97 | Wall | | 5 | | | x | x | |
| 12 July | 109 | Wall | | 6 | | x | x | x | |
| 13 July | 99 | Wall | | 6 | | x | x | x | |
| 12 July | 99 | Wall | | 6 | | x | | | |
| 03 May | 97 | Wall | | 7 | | x | x | x | |
| 12 July | 113 | Wall | | 7 | | x | x | x | |

strip chart, was found to be 56 mmHg, which represents approximately 19% of the mean pressure level in the test section over the period of the test.

Figures 4 through 15 contain the harmonic analysis records for each axial survey of the four radial positions; hub, mean, tip and outer casing wall. Some general observations can be made from a cursory examination of these figures. In all cases, the primary portion of the disturbance energy is associated with the frequency ratio, m = 23, at Port 5. In the successive downstream locations, the amplitude associated with blade passing frequency is seen to diminish rapidly.

The exact details of the spectra at different radial locations are varied. One noticeable trend in the tip radius harmonic analysis is a shift to higher frequencies of the dominant energy content as the fluid moves downstream. At all of the other radial locations, there tends to be an averaging of the amplitudes over all frequency ratios at successive axial locations. The significance of this frequency shift will be discussed in a later section.

The change with axial location of the amplitude of individual frequency ratios is shown in Figures 16 through 25. Each curve on the graphs is labeled with the frequency ratio it represents. The plots were constructed by selecting an arbitrary level for the amplitude for each harmonic analysis and then measuring the amplitude of frequencies whose value was greater than the preselected reference level. These dominant frequencies were selected at both Port 5 and at Port 7. The respective graphs indicate the results. It is seen that with the exception of blade passing frequency (m = 23), the behavior of the amplitude for different frequency ratios is varied. The results fall into two broad categories:

a) Those with amplitudes which either increase or decrease with axial location, and

b) Those with oscillating amplitudes which exhibit either a maximum or a minimum value at Port 6.

After examining the figures, it is apparent that few general conclusions can be made regarding the behavior of amplitude with respect to frequency ratio. The only repeatable patterns are those for m = 23, 6, and 1. In all cases, the amplitude associated with blade passing frequency (m = 23) is seen to decay rapidly. Frequency ratios of 6 and 1 are seen to exhibit the opposite behavior: their amplitudes increase as the flow progresses downstream. In an attempt to generalize these results, a graph was made to show the change in power with axial location for each frequency ratio which was selected as dominant at Port 7. This average was made from all the harmonic analysis data. The frequency ratios were averaged about integer values of m and were weighted to compensate for different numbers of samples at each integer m. The graph is shown in Figure 26. The results indicate that between Ports 5 and 6, the amplitude of frequency ratios greater than about 9 diminish while the low frequencies (m < 9) experience an increase in amplitude. The general trend betwenn Ports 6 and 7 is an overall averaging of the amplitudes for all frequency ratios.

Tracings were made of the harmonic analysis charts to smooth out some of the small scale randomness. The results appear in Figures 27

through 30. When viewed in this manner, certain trends which were vaguely indicated in the harmonic analysis records become much more pronounced. Figure 27 shows the spectrum for the hub radial position. At Port 5, several distinct peaks in amplitude are noticed. These correspond to frequency ratios of 1, 6, 12, 23 and 30. At Port 6, the amplitude for all frequency ratios is nearly constant with the exception of a peak at m = 6. Port 7 shows an overall increase in the average value of amplitude with peaks developing for frequency ratios between 6 and 20.

The corresponding figure for the mean radius shows peaks at m = 2, 6, and 23 at Port 5. The trend at Port 6 is again an increase in the energy associated with frequencies for $m < 9$ and an overall decay for $m > 9$. Port 7 displays an averaging with m's between 9 and 14, attaining a level comparable to the $m < 9$ level.

The tip data are by far the most interesting. As the flow progresses from Port 5 to Port 7, very distinct peaks develop at m = 2, 6, and 12, in addition to the increasing frequency associated with the peak of the spectrum (m = 23 to 27). Figure 31 shows the behavior of this shifting peak in the power spectrum.

The wall static tracings exhibit behavior very similar to that at the mean radius. One startling difference between the wall static data and the tip radius data is the complete absence of a shifting frequency associated with the peak of the power spectrum. In fact, it is only at the tip radius that a large percentage of the disturbance energy remains clustered about a particular frequency at Ports 6 and 7. In all other cases, the peak associated with blade passing decays rapidly. This result will be elaborated upon in a subsequent section. The tracings verify the type of

behavior indicated by the graph of average change in power between axial locations (Fig. 26).

One last form of data presentation was explored. Evans [1] indicates that blade passing frequency and its harmonics are the only significant sources of disturbance energy in the spectrum. To investigate this result, the range of the frequency spectrum analyzed was extended to include the first two harmonics of blade passing. The harmonic analyses were again carried out at each axial survey of the hub, mean, and tip radial locations. The results are presented in Figures 32 through 40. At the mean radius, the harmonics of blade passing frequency are the frequencies associated with the largest portion of the disturbance at Port 5. At Port 6, only blade passing frequency remains and at Port 7, even this frequency has decayed to the mean amplitude. The corresponding hub data shows only blade passing frequency dominant at Port 5. By Port 6, this amplitude has decayed to the mean level. The tip radius data shows blade passing frequency and its harmonics at Port 5. The frequency corresponding to m = 25.0 is dominant at Port 6, and at Port 7, it is only the frequency for m = 26.5 which remains.

## 4.2 Theoretical Predictions

Kerrebrock [5] suggests that a better comprehension of turbomachine flows should follow from a clearer understanding of the behavior of all the small disturbances in the rotating flow field of a turbomachine. In uniform flow, these disturbances may be classified into three types: pressure, vorticity, and entropy. In flows with strong rotation, these three types of small disturbances are not independent of each other. A radial or tangential velocity perturbation or a density fluctuation, implies a radial

or coriolis force perturbation which leads to a pressure fluctuation, thus coupling the vorticity and entropy modes to the pressure mode.

Pressure disturbances can originate from any of a number of disturbances of the radial equilibrium in a swirling, non-uniform flow. The types of disturbances which occur in non-rotating flows should occur, though perhaps with some modifications, in rotating flows. These should include propagating pressure waves and some purely convected shear and entropy disturbances. In addition, there should be disturbances unique to rotating flows.

The results of Kerrebrock's work show that the behavior of the pressure mode in the strongly swirling flow will not be significantly different from that in a non-rotating flow. The pure shear mode for the free vortex velocity distribution may contain radial and axial fluctuations, but no tangential fluctuations. These fluctuations are pressure free and purely convected. In the free vortex, it appears that the shear field is completed by shear induced waves which are purely convected at some radius but propagate elsewhere. These waves have rather strong pressure fluctuations associated with them.

Kerrebrock concludes that in rotating flows, shear disturbances are associated with oscillating pressure fields, the amplitudes of which are comparable to those of the sound mode provided that the potential flow and shear velocity are comparable.

# CHAPTER V

## CONCLUSIONS

As expected, the major portion of the disturbance energy directly behind the rotor is attributable to the viscous wakes. In the successive downstream ports, the large amount of energy initially associated with the wakes is transferred to other frequency ratios, primarily those with $m < 9$ at Port 6. The mixing and decay process continues until at Port 7 the entire frequency spectrum has been smoothed to an average energy level.

Two distinct patterns of amplitude behavior are found to exist in the downstream flow. Some frequencies have amplitudes which are either attenuated or amplified as they move downstream, while other frequencies have amplitudes which appear to be oscillatory. No generalization concerning a correlation between frequency ratio and the type of amplitude behavior observed is apparent.

The shift in the peak of the power spectrum to higher frequency ratios as the flow moves downstream is suggested to be the result of the wakes being centrifuged outward. The rotor blading is designed for a free vortex velocity distribution. If the wakes conserve angular momentum as they move radially outward, then they will have a tangential velocity excess as they move towards the tip. This additional velocity causes the overall tip flow field to spin faster as it moves downstream. If it is supposed that the viscous wake disturbance is fixed in the fluid field, then spinning the fluid faster will result in an increase in the frequency of the disturbance. It is suggested that the shifting frequency ratio associated with the power peak observed in the tip data is actually the viscous wakes

being convected downstream in a fluid which has increasing swirl velocity as it travels away from the rotor.

The apparent discrepancy in the tip and wall static data regarding this shifting frequency may tentatively be explained as follows. The wall static measurements are made directly at the outer casing wall. This insures that the radial velocity be zero. The pressure fluctuations recorded by the wall transducers are, therefore, due to acoustical disturbances which propagate downstream. The tip radius data on the other hand is measured 1/2 inch from the outer casing where strong radial flows are known to exist. If as suggested the wakes and their accompanying tangential velocity excess are centrifuged to the outer radius, then the tip data will reflect this convected disturbance although the wall measurement will not. Further evidence supporting this conclusion is provided by one test in which the traverser failed to fire across the test section. The static pressure probe remained at the outer casing wall of Port 6 throughout the test. An harmonic analysis of this run showed a strong peak in amplitude at a frequency ratio of 26 (Fig. 41). This is the same phenomenon which is reflected in the Port 6 tip radius data. Because the static pressure probe is guided through the outer casing wall through a 5/8 inch diameter cavity, the probe did not record the same data as measured by the wall transducer, the reason apparently being that the zero radial velocity condition at the wall does not apply to the probe which is positioned within a cavity.

Another explanation, for the frequency shift, which must be considered is that the rotor's angular velocity decreases during the test time, so that fluid at Port 7 left the rotor when it had a higher angular velocity than it has at the time the pressure measurement is made. A simple calculation shows,

however, that the frequency shift due to this cannot exceed about 0.2 percent, whereas the observed shift is nearly 20 percent.

One last detail contributes to the theory of the wakes moving radially outward. At Port 5, the hub data (Fig. 27) shows amplitude peaks at m = 2, 6, and 12. An inspection of Figure 29 shows the same peaks are present in the Port 5 tip data. In fact, these peaks become more pronounced at Port 6 and 7 of the tip data, although they are not evident in the corresponding hub data. If these disturbances are indeed centrifuged outward and carry with them strong pressure fluctuations, then there should be evidence of them at the tip radius since the flux of these disturbances must be constrained by the outer casing.

The harmonic analysis of the extended frequency spectrum supports Evans' claim that blade passing frequency and its harmonics are the dominant disturbances behind the rotor, but it also shows a great deal of low frequency structure which was not resolved in his measurements.

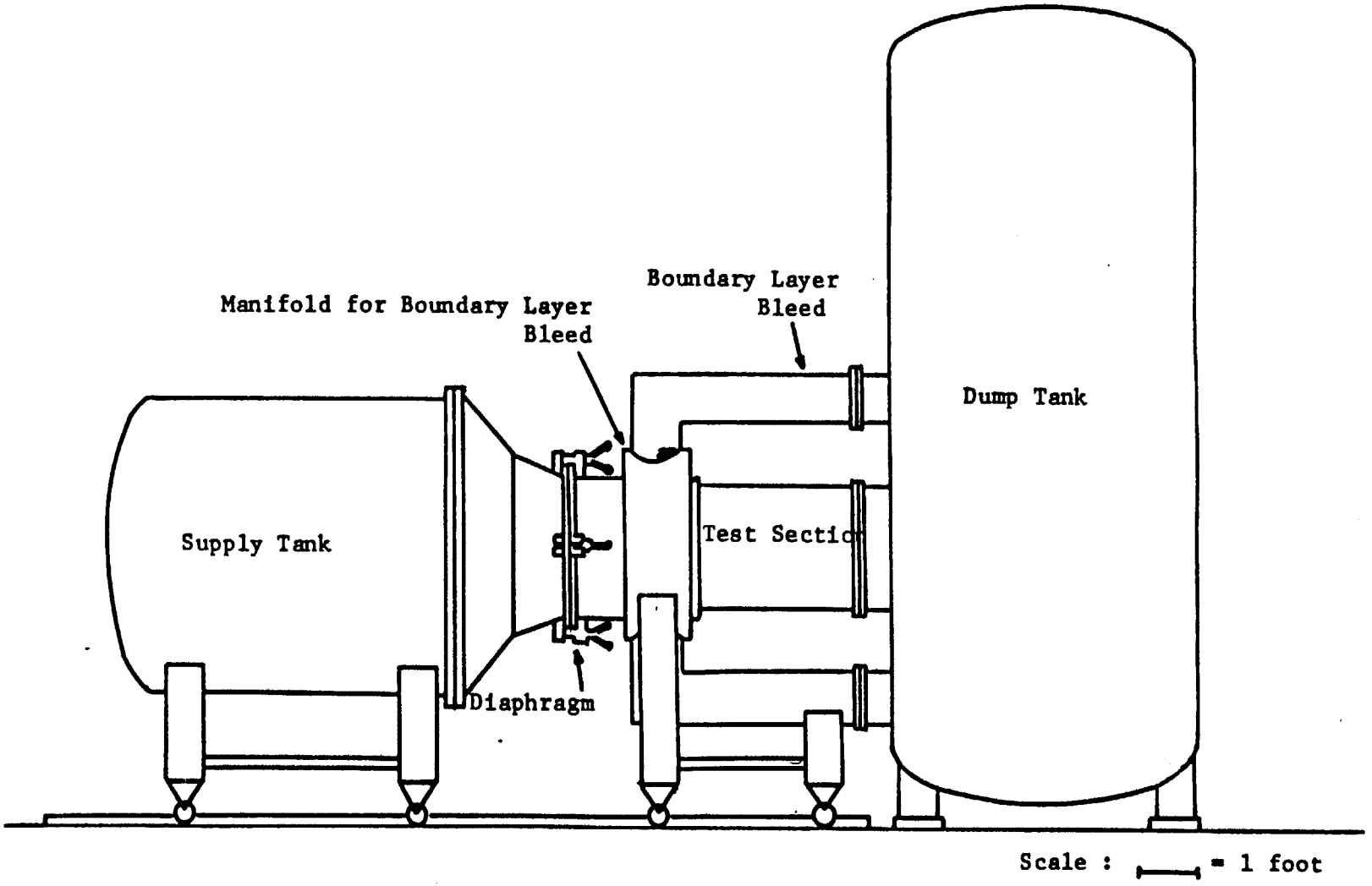


Figure 1

Scale drawing of Blowdown Compressor Facility,
sized for 23.25 inch diameter rotor

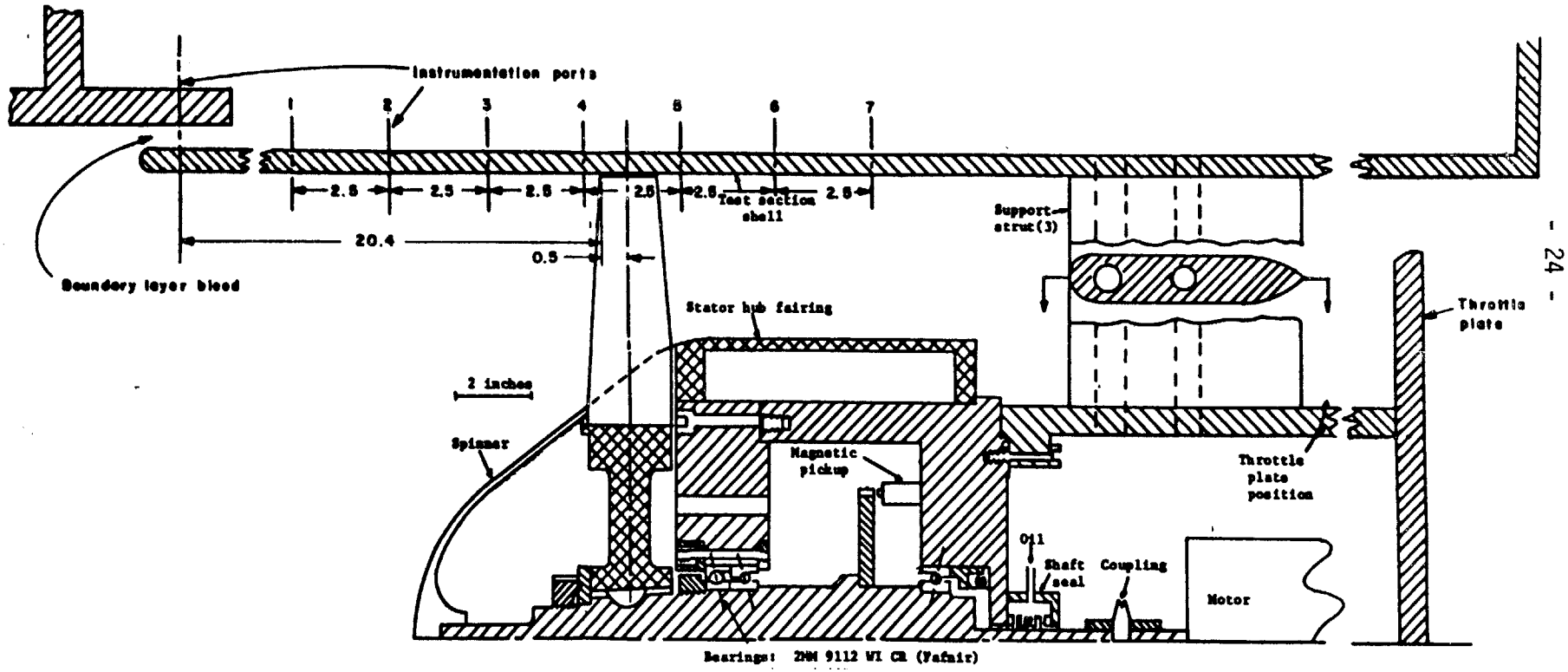
Instrumentation ports
1
2
3
4
5
6
7
2.5
2.5
2.5
2.5
2.5
Test section shell
2.5
20.4
0.5
Boundary layer bleed
Support strut (3)
Throttle plate
Stator hub fairing
2 inches
Spinner
Magnetic pickup
Throttle plate position
Oil
Shaft seal
Coupling
Motor
Bearings: 2MM 9112 WI CR (Fafnir)

FIGURE 2

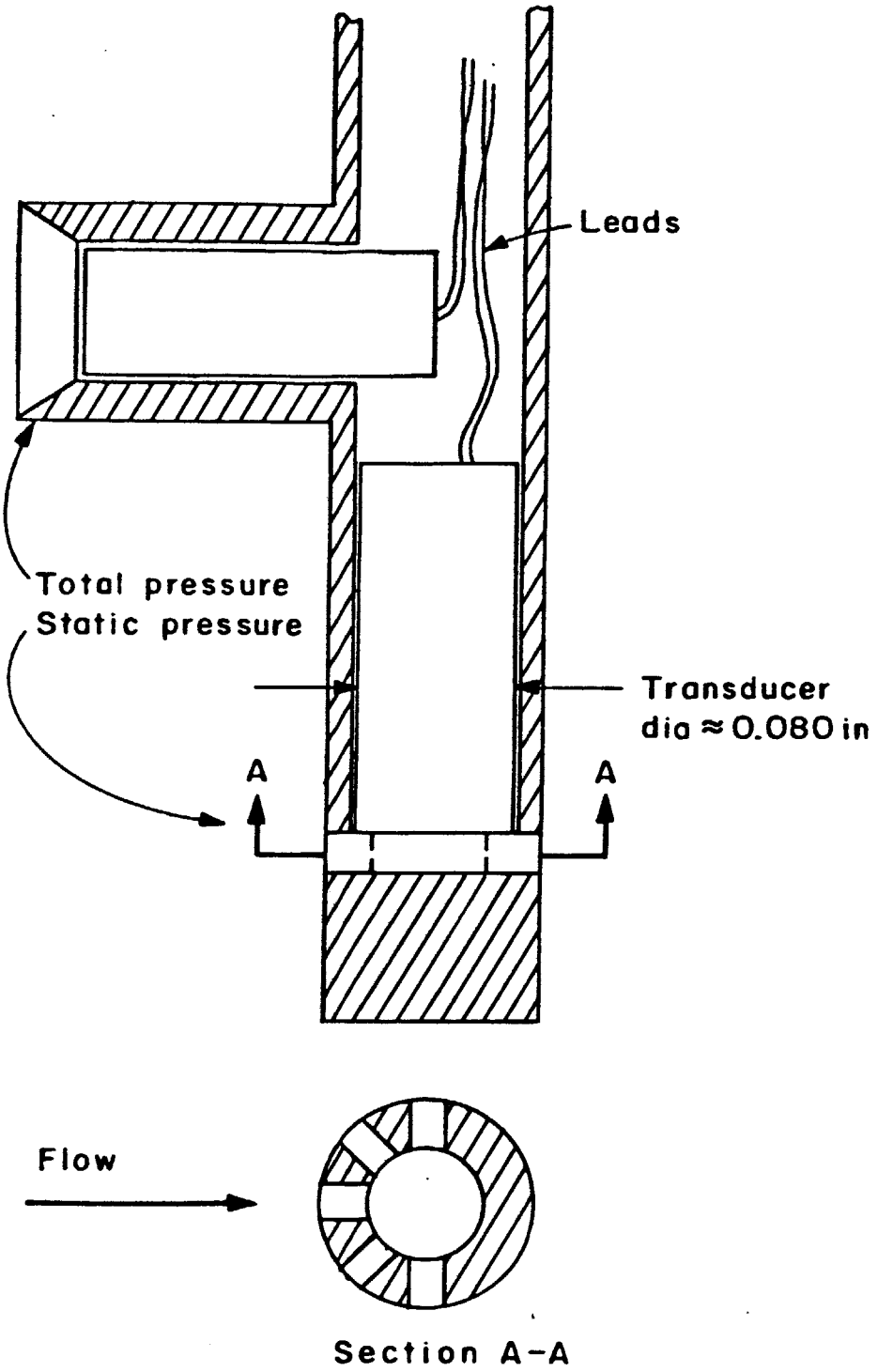


Figure 3: Combination probe used for surveys of stagnation and static pressure in flow field

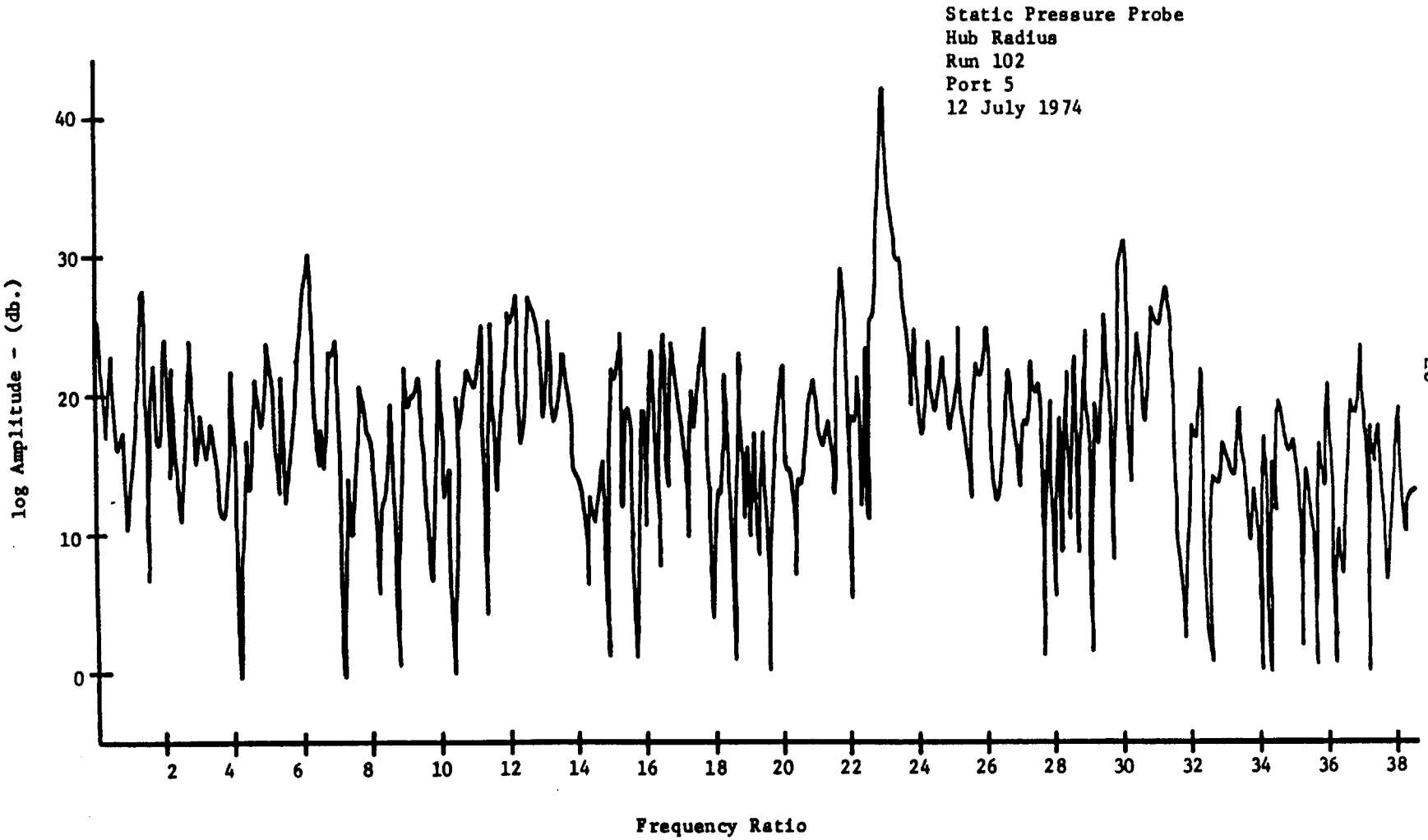
Static Pressure Probe
Hub Radius
Run 102
Port 5
12 July 1974
log Amplitude - (db.)
40
30
20
10
0
2
4
6
8
10
12
14
16
18
20
22
24
26
28
30
32
34
36
38
Frequency Ratio

Figure 4

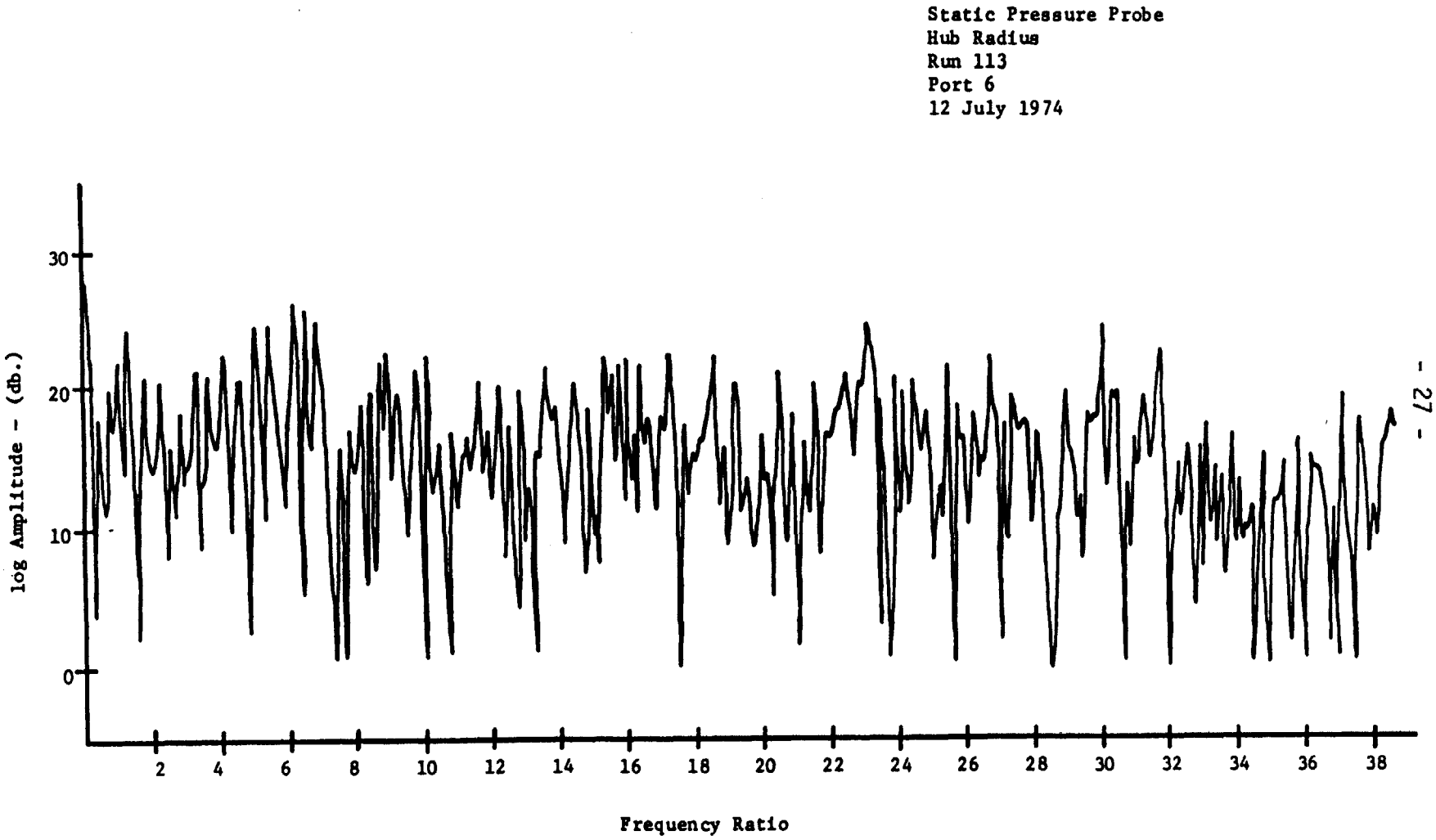
Static Pressure Probe
Hub Radius
Run 113
Port 6
12 July 1974
log Amplitude - (db.)
30
20
10
0
2
4
6
8
10
12
14
16
18
20
22
24
26
28
30
32
34
36
38
Frequency Ratio

Figure 5

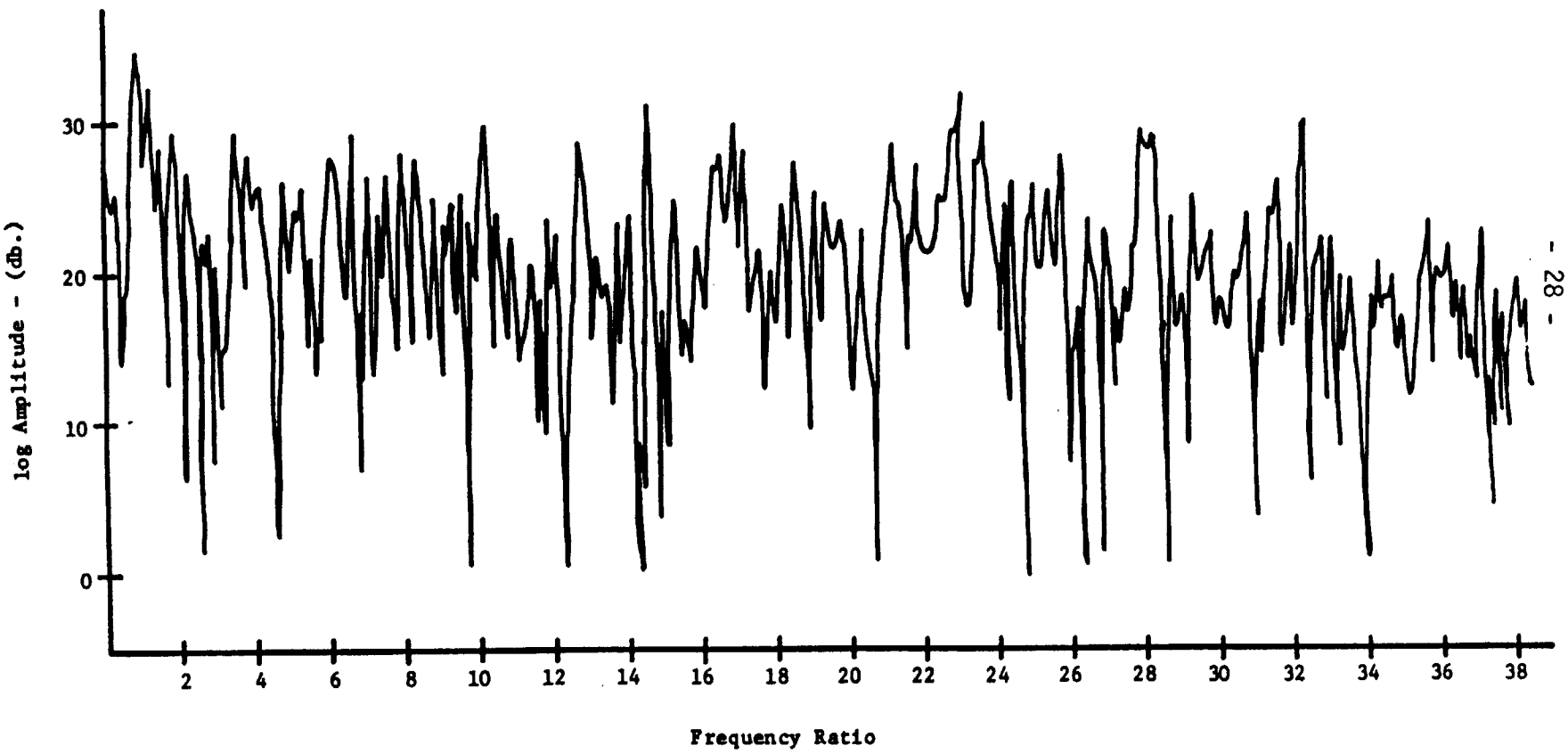
Static Pressure Probe
Hub Radius
Run 109
Port 7
11 July 1974
log Amplitude - (db.)
30
20
10
0
2
4
6
8
10
12
14
16
18
20
22
24
26
28
30
32
34
36
38
Frequency Ratio

Figure 6

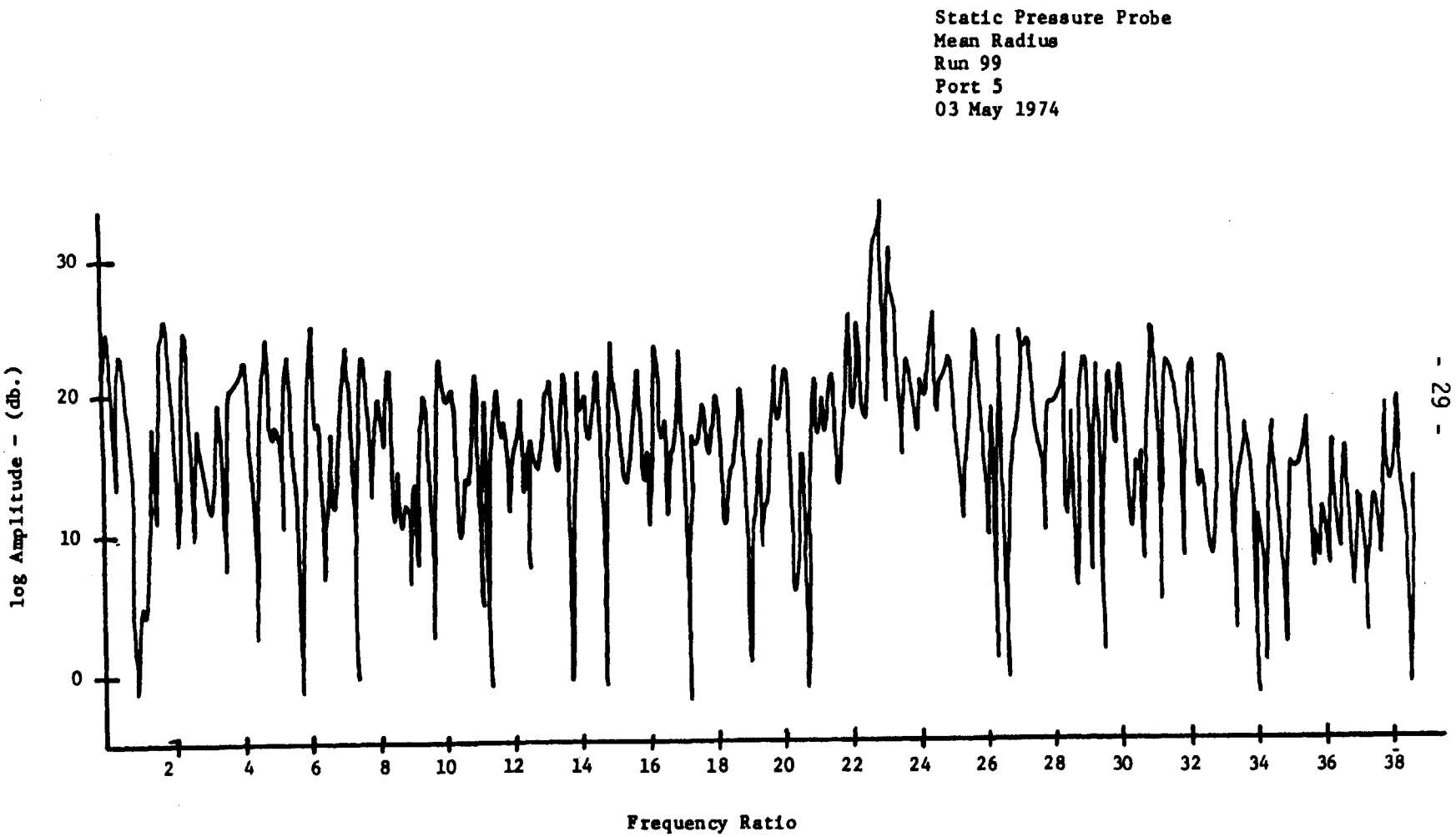
Static Pressure Probe
Mean Radius
Run 99
Port 5
03 May 1974
log Amplitude - (db.)
30
20
10
0
2
4
6
8
10
12
14
16
18
20
22
24
26
28
30
32
34
36
38
Frequency Ratio

Figure 7

Static Pressure Probe
Mean Radius
Run 97
Port 6
03 May 1974

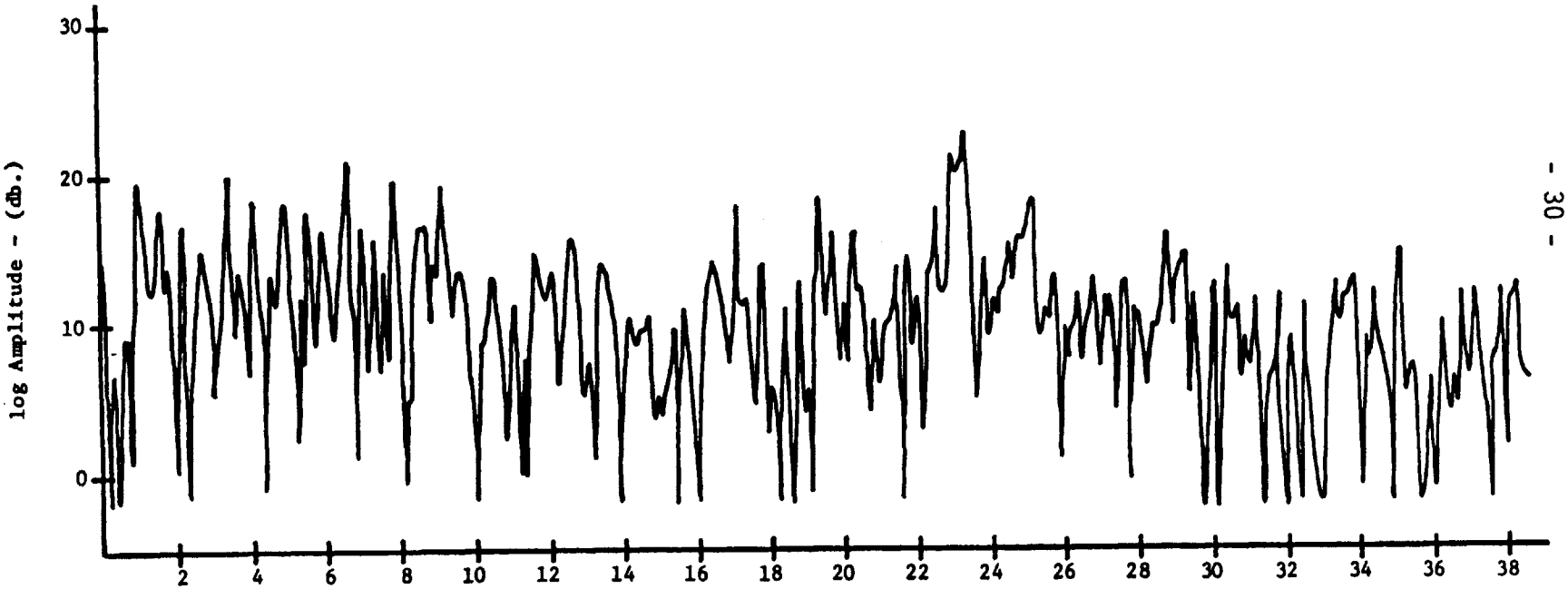


Figure 8

Static Pressure Probe
Mean Radius
Run 98
Port 7
03 May 1974

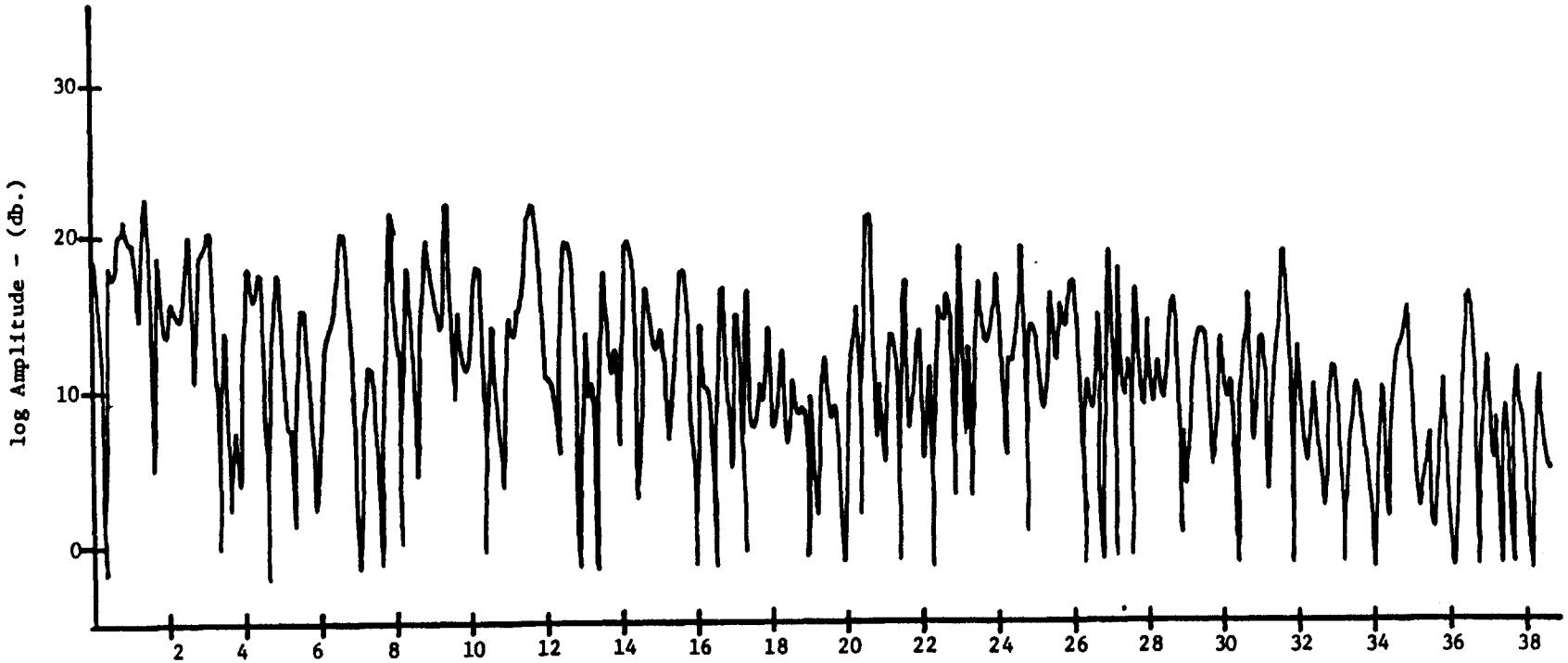


Figure 9

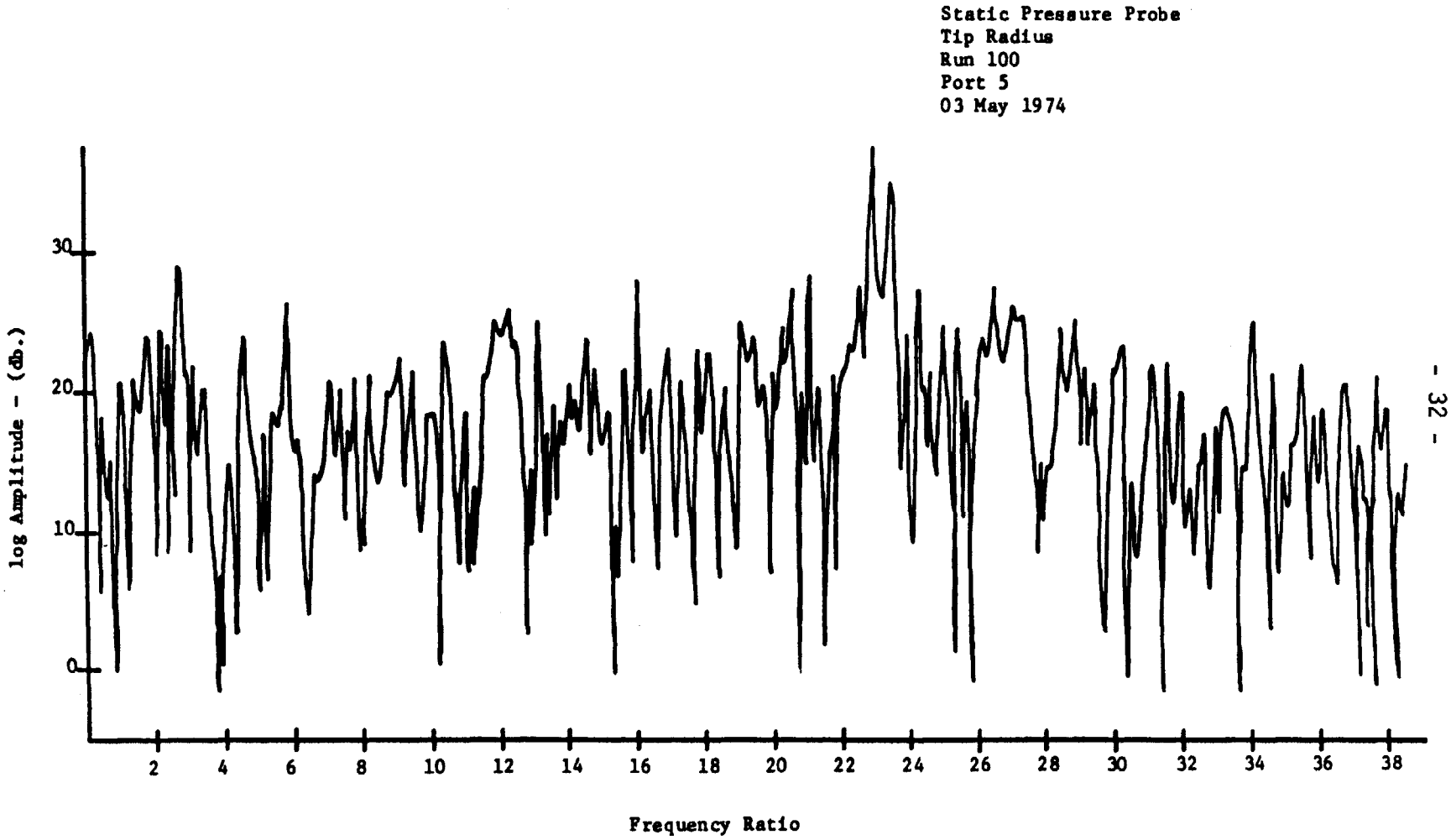
Static Pressure Probe
Tip Radius
Run 100
Port 5
03 May 1974
log Amplitude - (db.)
30
20
10
0
2
4
6
8
10
12
14
16
18
20
22
24
26
28
30
32
34
36
38
Frequency Ratio

Figure 10

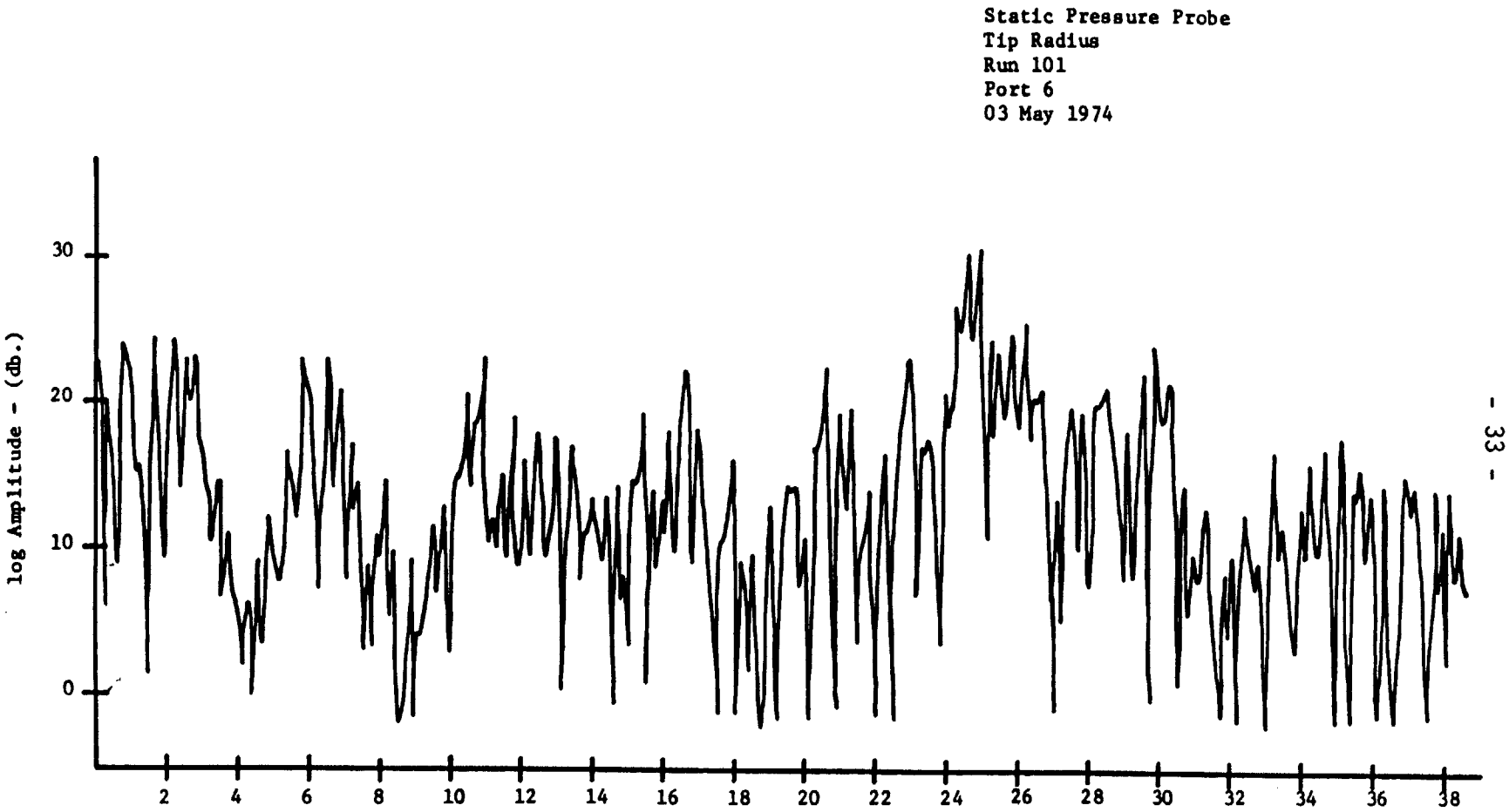
Static Pressure Probe
Tip Radius
Run 101
Port 6
03 May 1974
log Amplitude - (db.)
30
20
10
0
2
4
6
8
10
12
14
16
18
20
22
24
26
28
30
32
34
36
38
Frequency Ratio

Figure 11

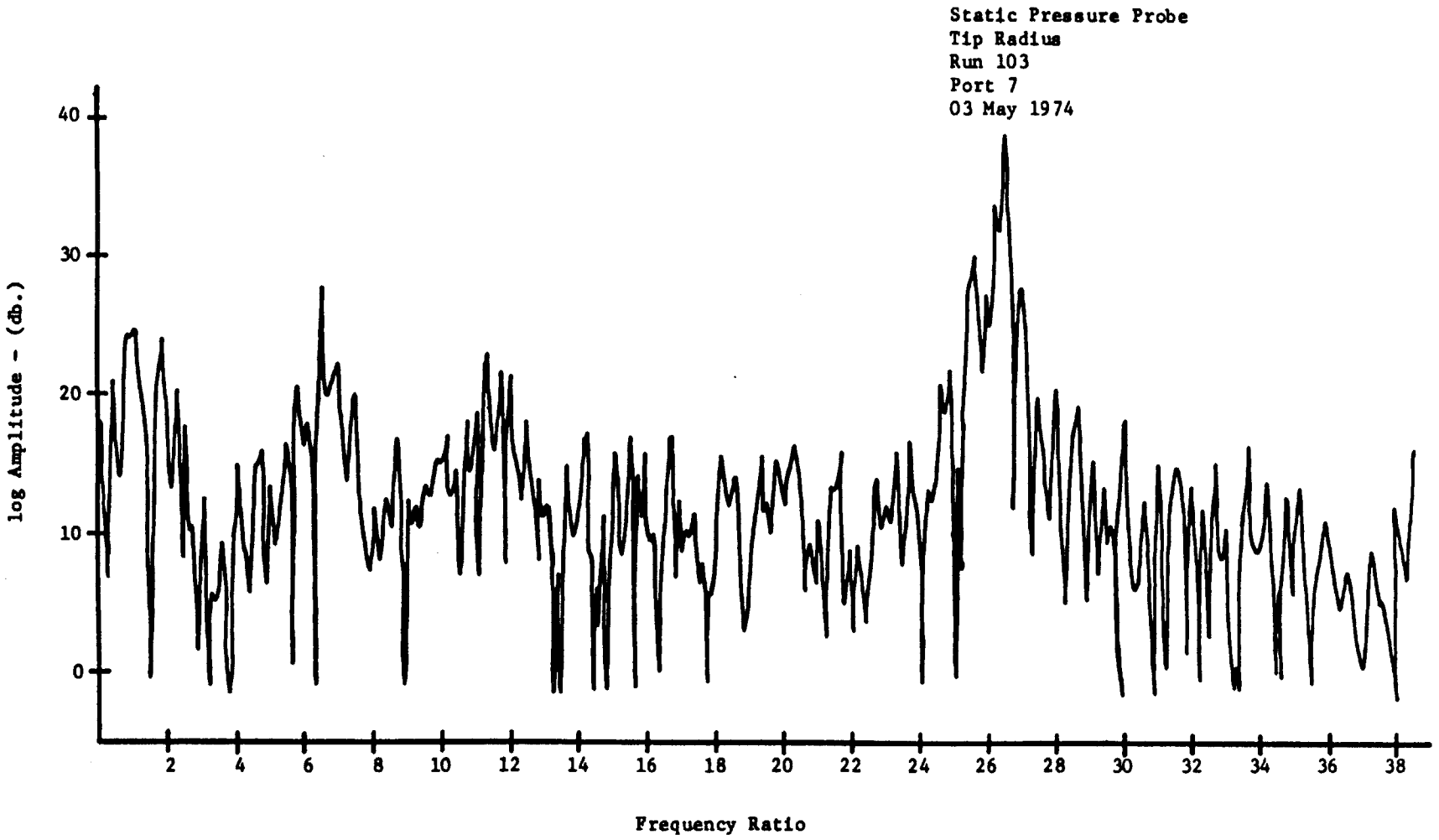
Static Pressure Probe
Tip Radius
Run 103
Port 7
03 May 1974
log Amplitude - (db.)
40
30
20
10
0
2
4
6
8
10
12
14
16
18
20
22
24
26
28
30
32
34
36
38
Frequency Ratio

Figure 12

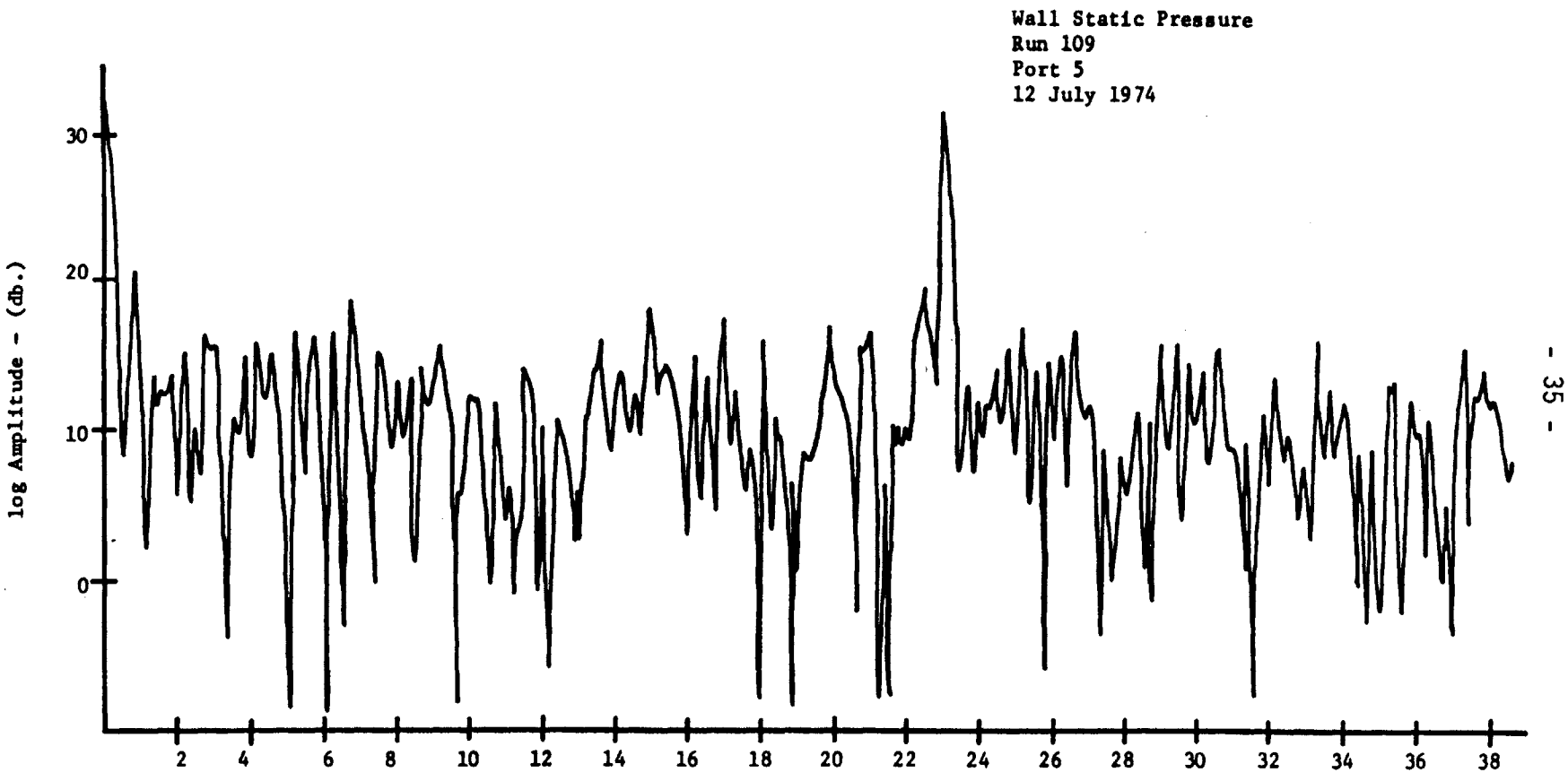
Wall Static Pressure
Run 109
Port 5
12 July 1974
log Amplitude - (db.)
30
20
10
0
2
4
6
8
10
12
14
16
18
20
22
24
26
28
30
32
34
36
38
Frequency Ratio

Figure 13

Wall Static Pressure
Run 99
Port 6
13 July 1974

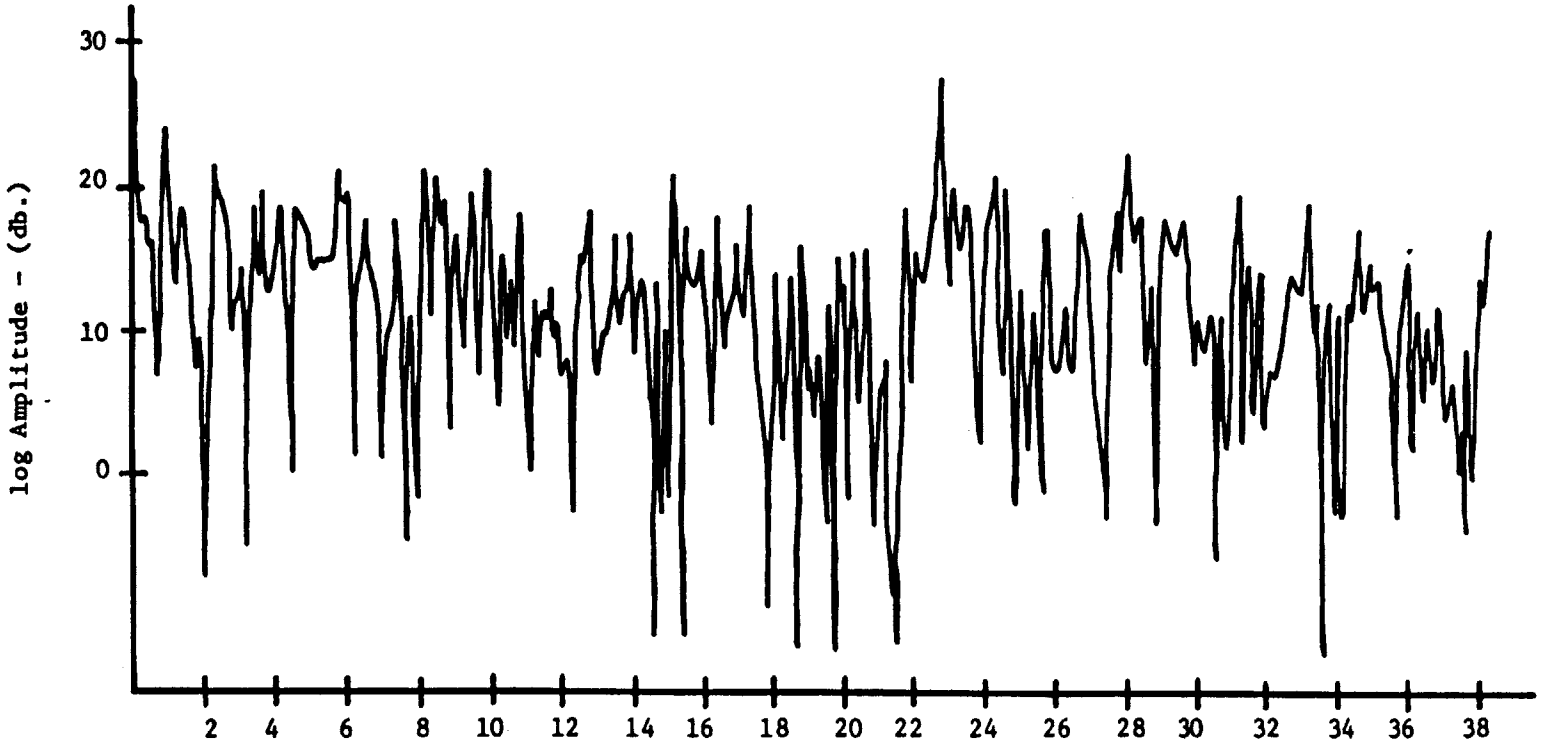


Figure 14

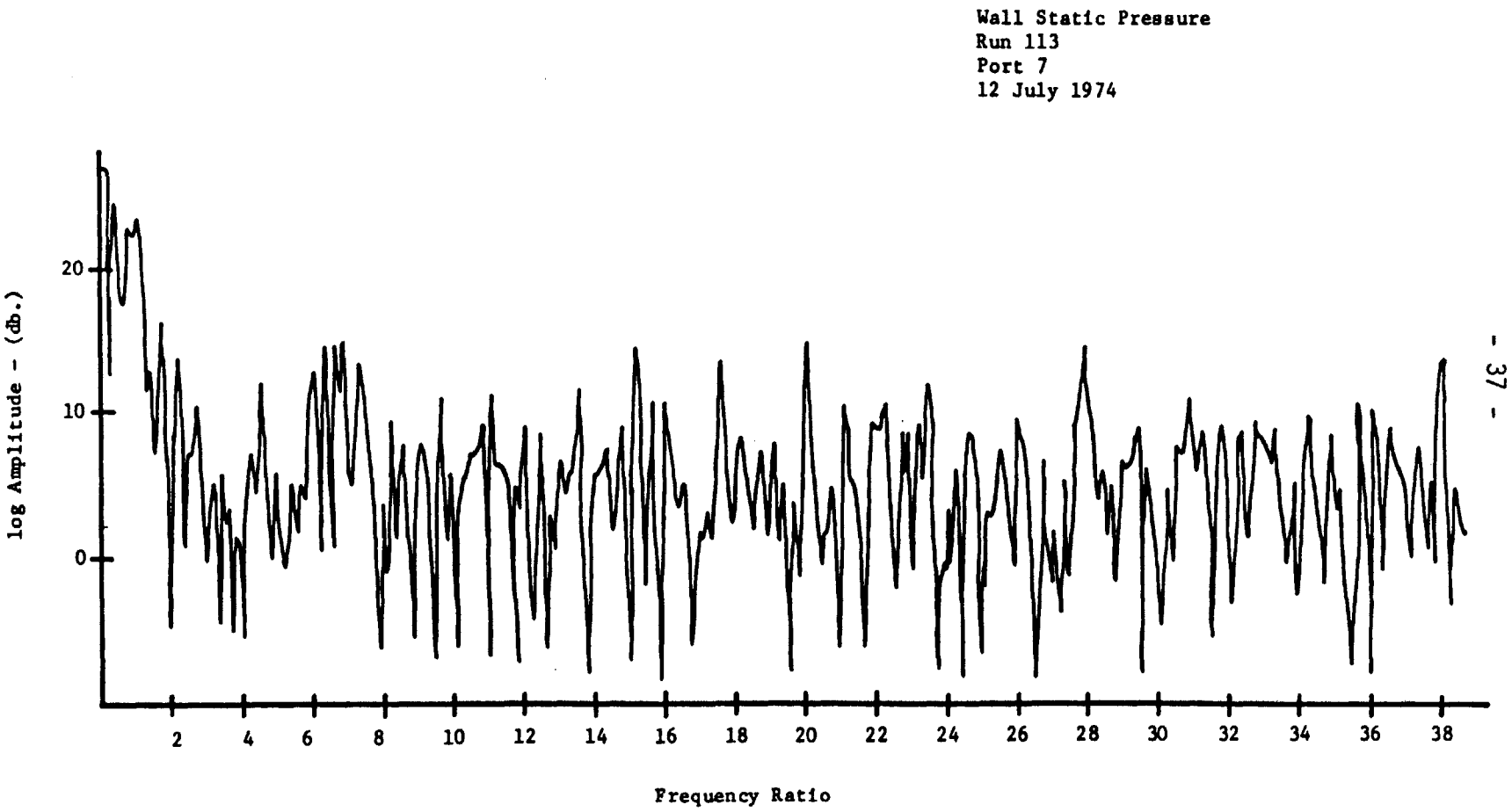
Wall Static Pressure
Run 113
Port 7
12 July 1974
log Amplitude - (db.)
20
10
0
2
4
6
8
10
12
14
16
18
20
22
24
26
28
30
32
34
36
38
Frequency Ratio

Figure 15

Static Pressure Probe
Hub Radius
Frequency Dominant at Port 7
Data: 11, 12 July 1974
Plot: 19 July 1974

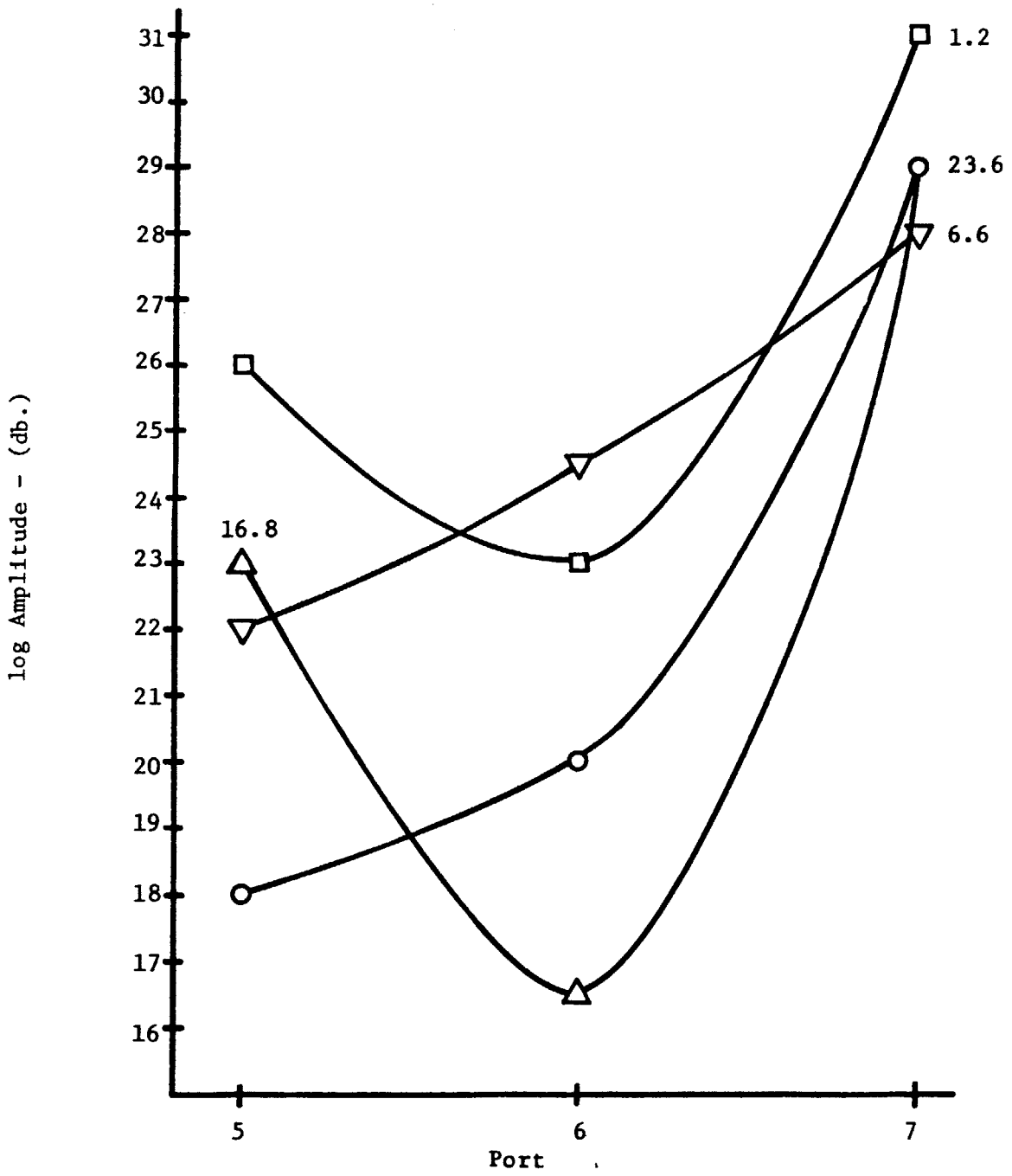


Figure 16

Static Pressure Probe
Hub Radius
Frequency Dominant at Port 7
Data: 11, 12 July 1974
Plot: 19 July 1974

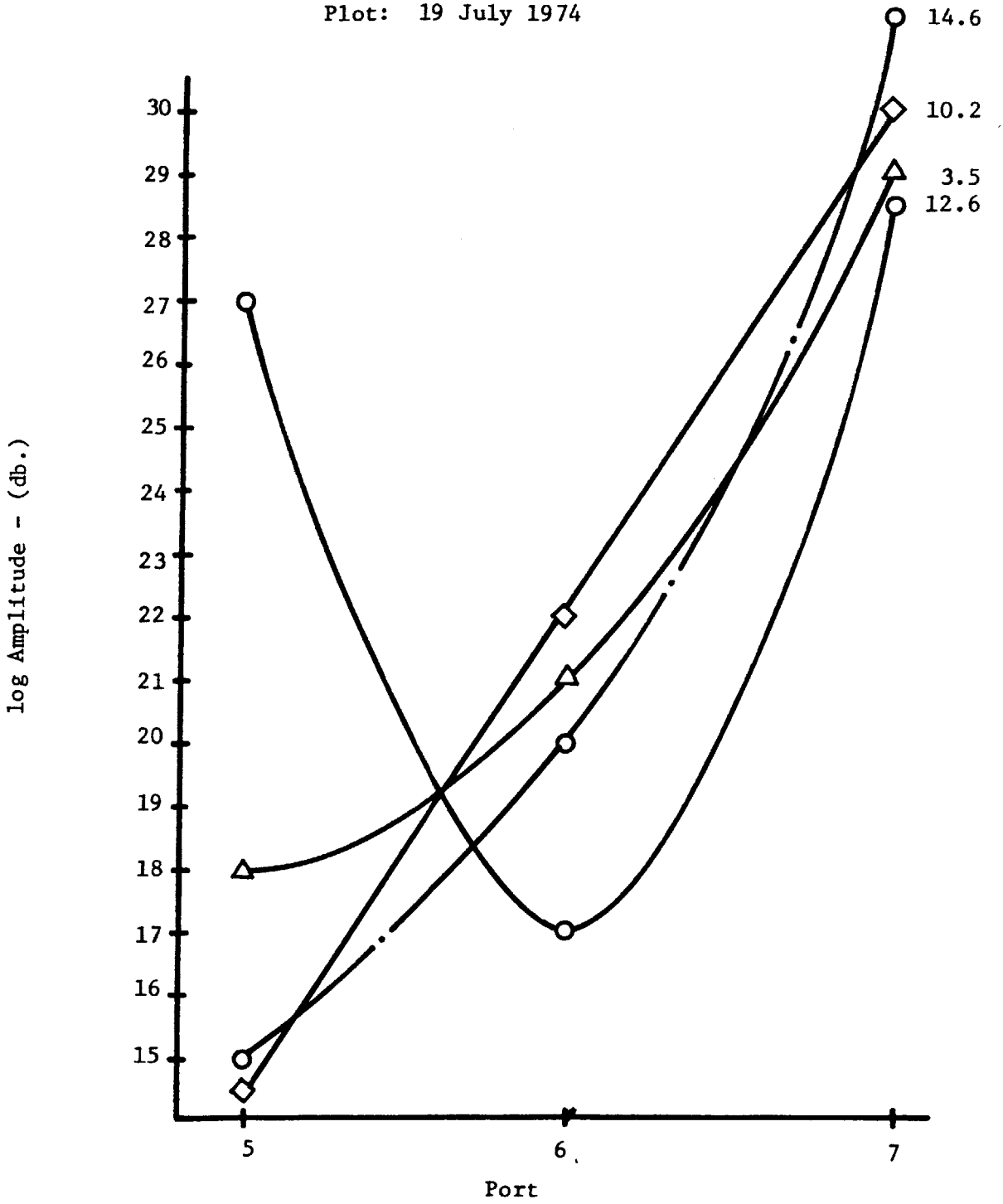


Figure 17

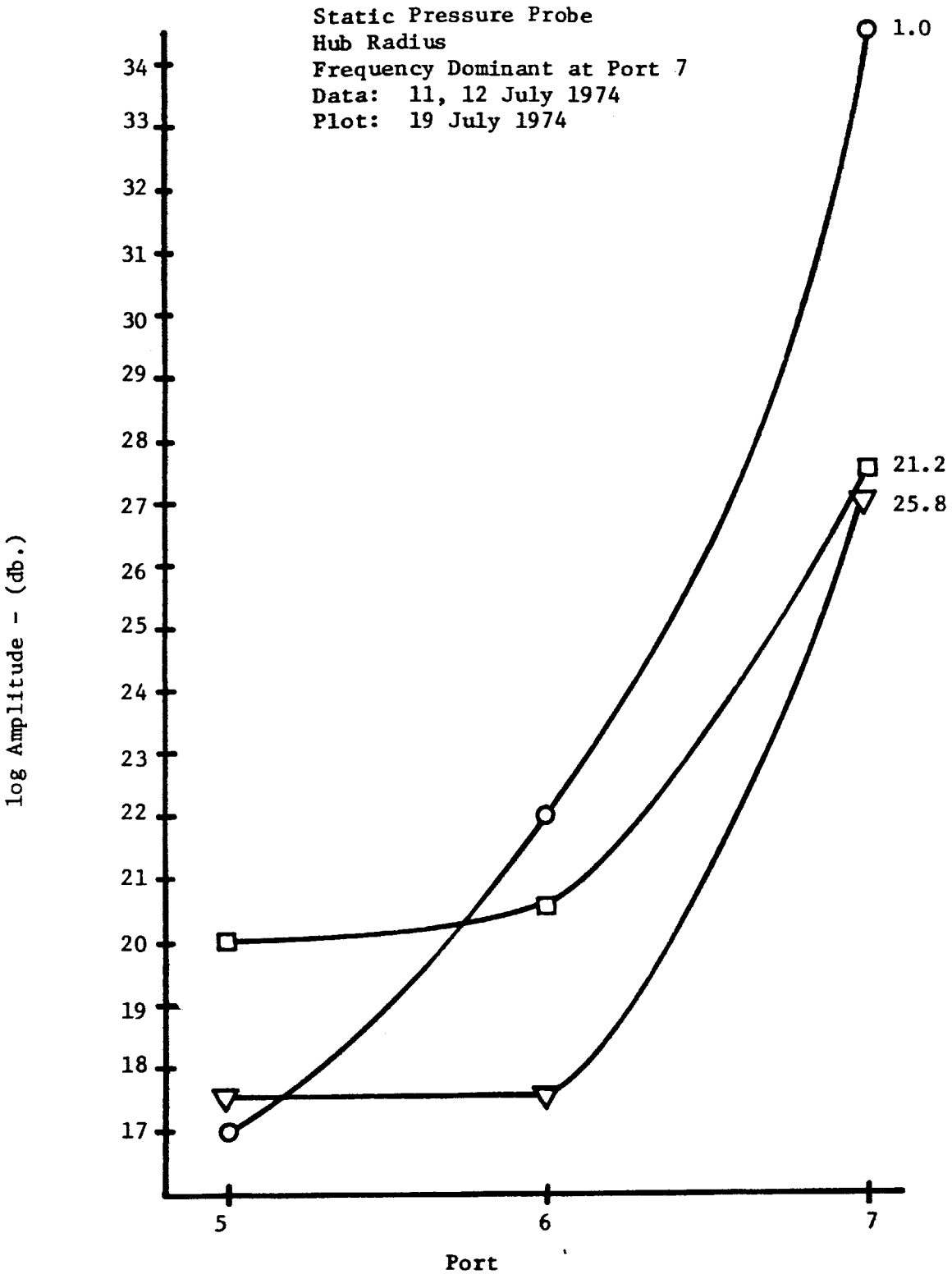
Static Pressure Probe
Hub Radius
Frequency Dominant at Port 7
Data: 11, 12 July 1974
Plot: 19 July 1974
1.0
21.2
25.8
log Amplitude - (db.)
34
33
32
31
30
29
28
27
26
25
24
23
22
21
20
19
18
17
5
6
7
Port

Figure 18

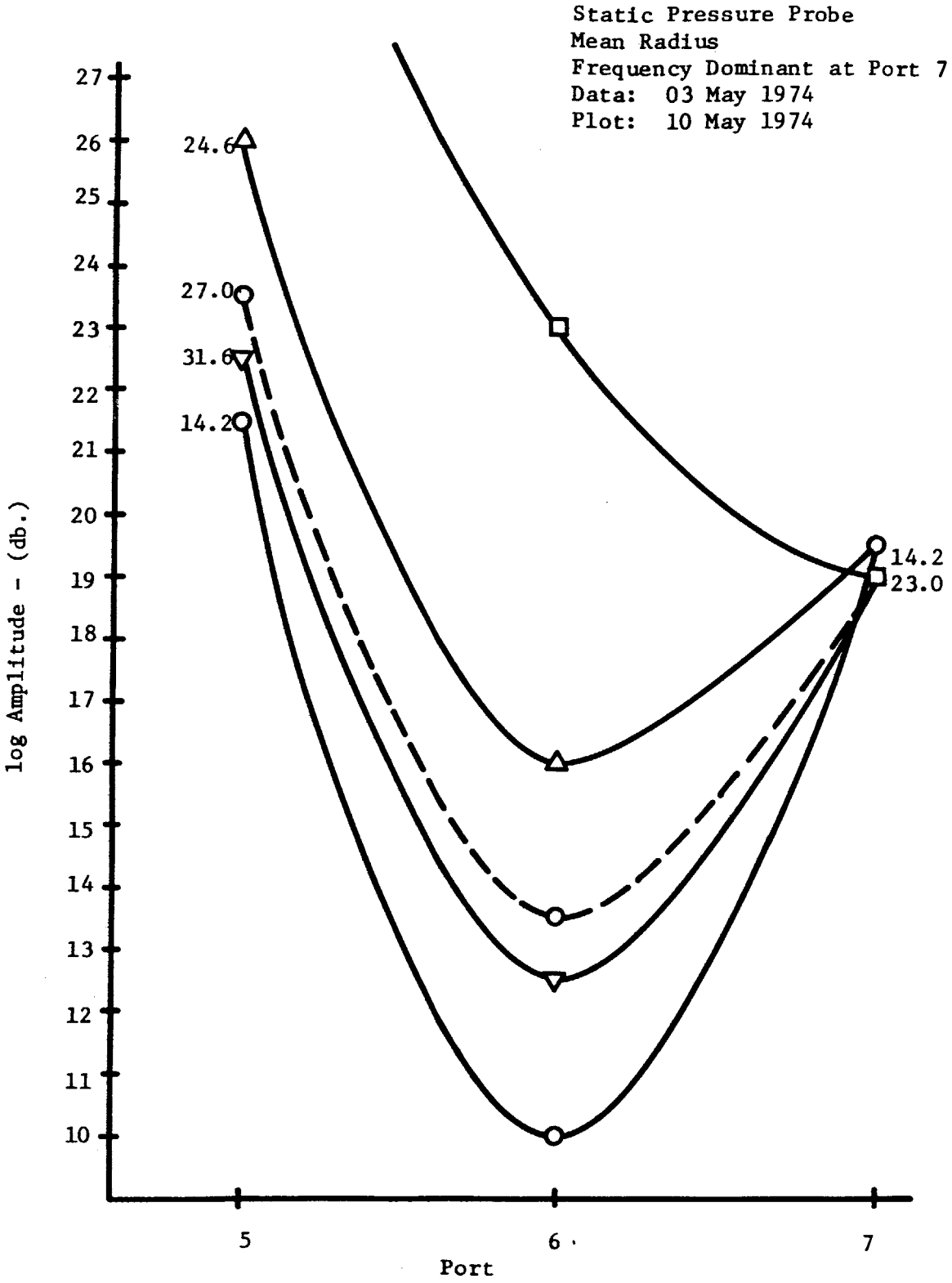
Static Pressure Probe
Mean Radius
Frequency Dominant at Port 7
Data: 03 May 1974
Plot: 10 May 1974
log Amplitude - (db.)
27
26
25
24
23
22
21
20
19
18
17
16
15
14
13
12
11
10
24.6
27.0
31.6
14.2
14.2
23.0
5
6
7
Port

Figure 19

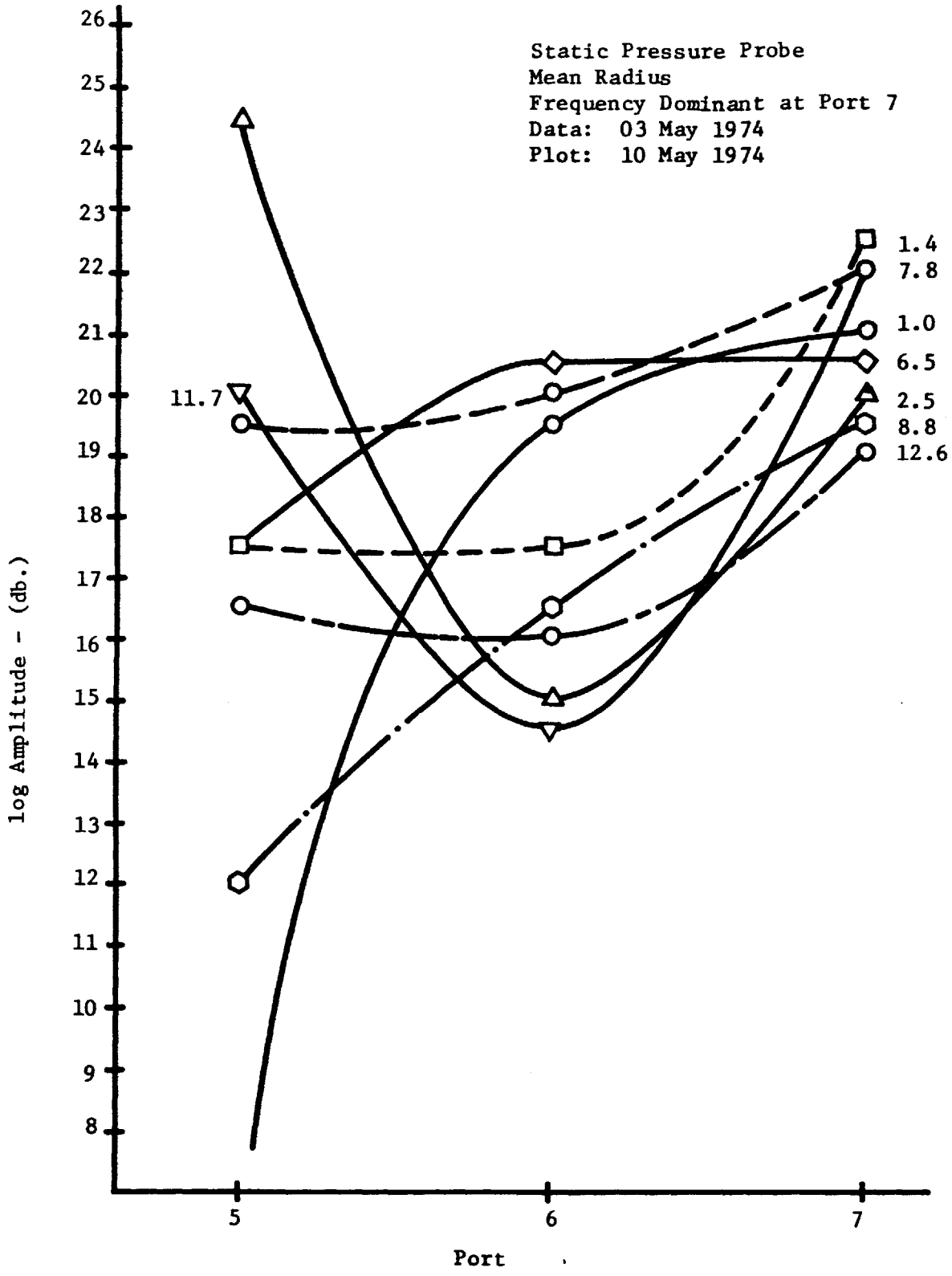
Static Pressure Probe
Mean Radius
Frequency Dominant at Port 7
Data: 03 May 1974
Plot: 10 May 1974
log Amplitude - (db.)
26
25
24
23
22
21
20
19
18
17
16
15
14
13
12
11
10
9
8
5
6
7
Port
1.4
7.8
1.0
6.5
11.7
2.5
8.8
12.6

Figure 20

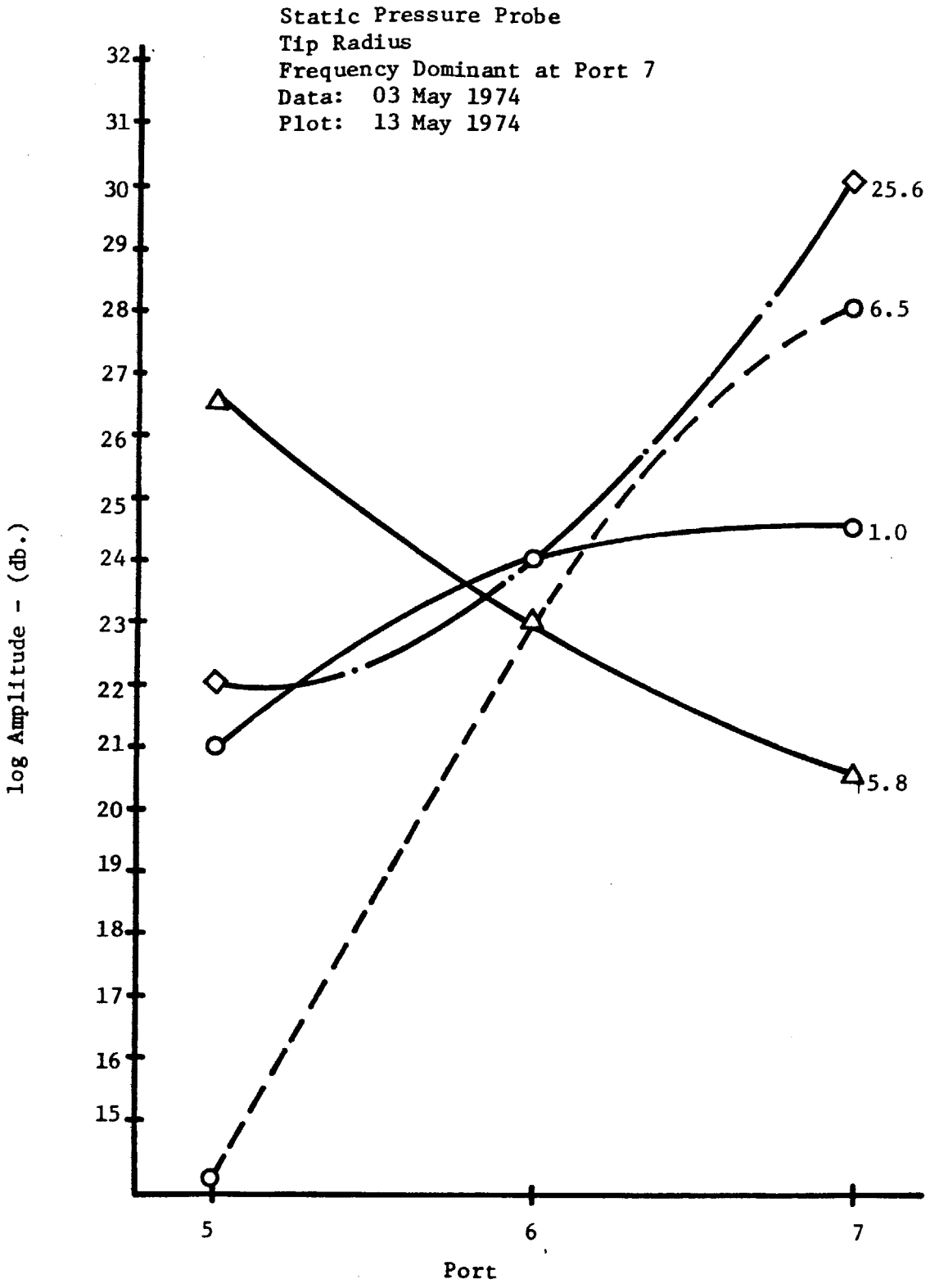
Static Pressure Probe
Tip Radius
Frequency Dominant at Port 7
Data: 03 May 1974
Plot: 13 May 1974
log Amplitude - (db.)
32
31
30
29
28
27
26
25
24
23
22
21
20
19
18
17
16
15
25.6
6.5
1.0
5.8
5
6
7
Port

Figure 21

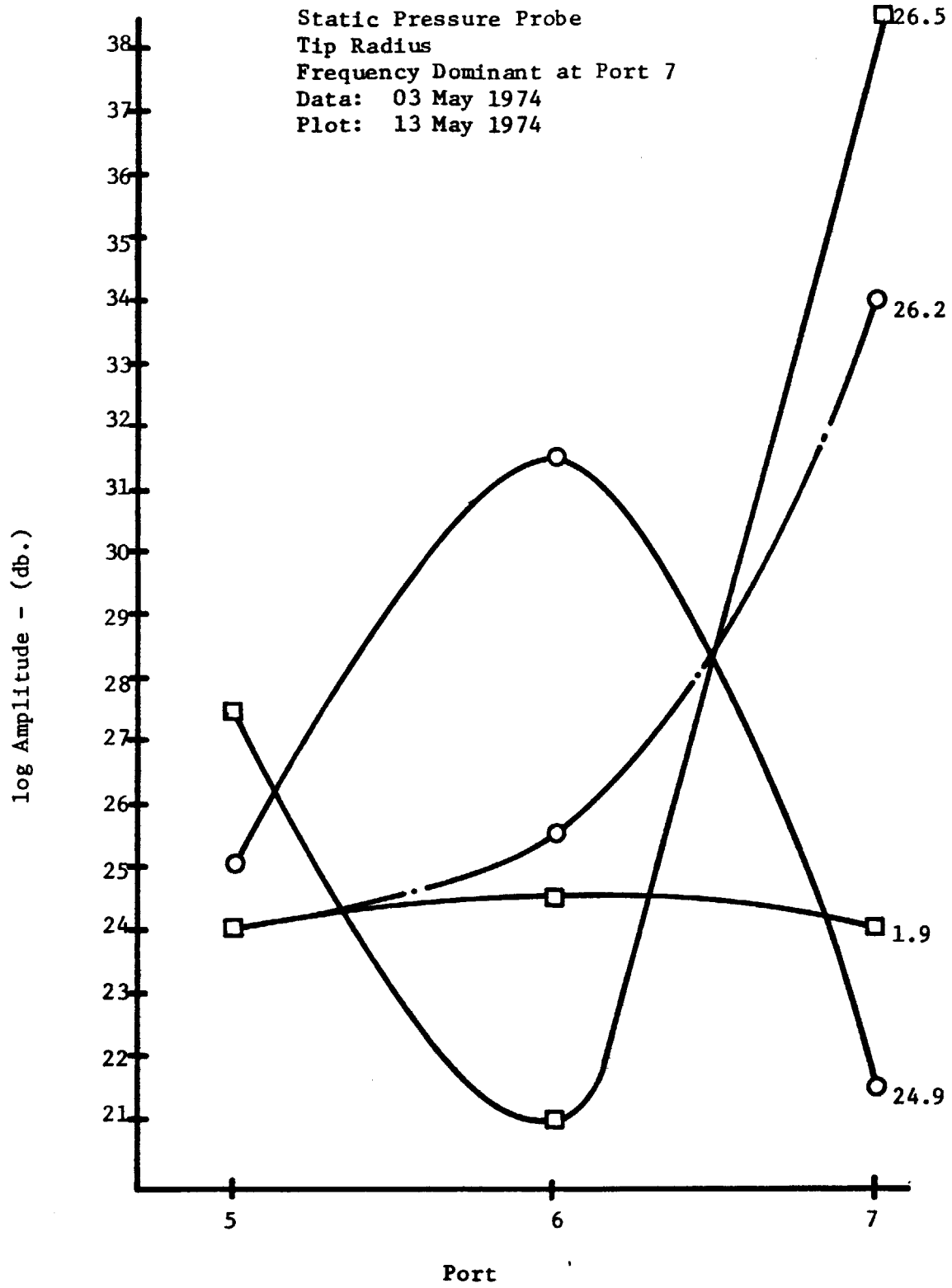
Static Pressure Probe
Tip Radius
Frequency Dominant at Port 7
Data: 03 May 1974
Plot: 13 May 1974
26.5
26.2
1.9
24.9
38
37
36
35
34
33
32
31
30
29
28
27
26
25
24
23
22
21
log Amplitude - (db.)
5
6
7
Port

Figure 22

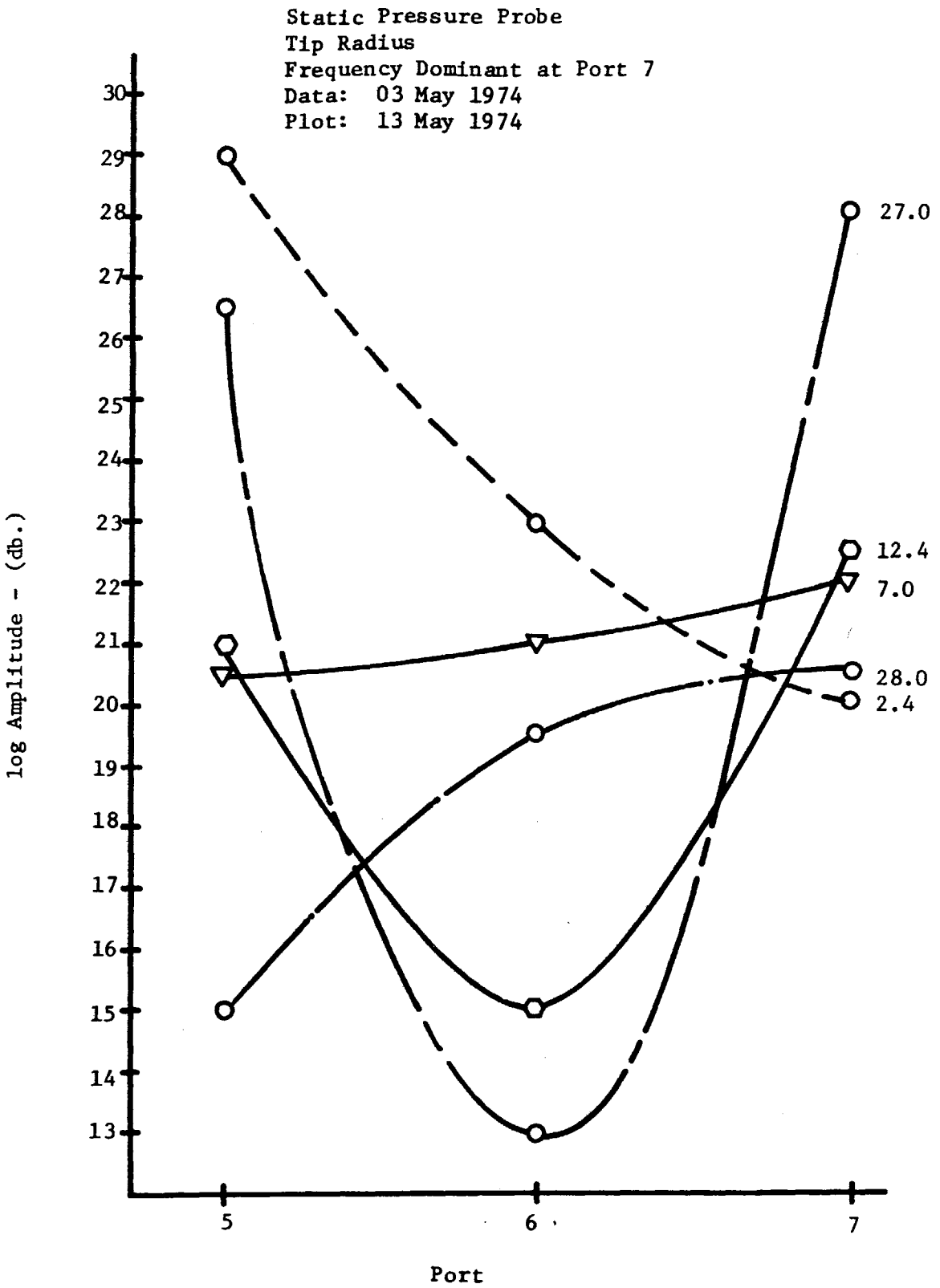
Static Pressure Probe
Tip Radius
Frequency Dominant at Port 7
Data: 03 May 1974
Plot: 13 May 1974
log Amplitude - (db.)
30
29
28
27
26
25
24
23
22
21
20
19
18
17
16
15
14
13
27.0
12.4
7.0
28.0
2.4
5
6
7
Port

Figure 23

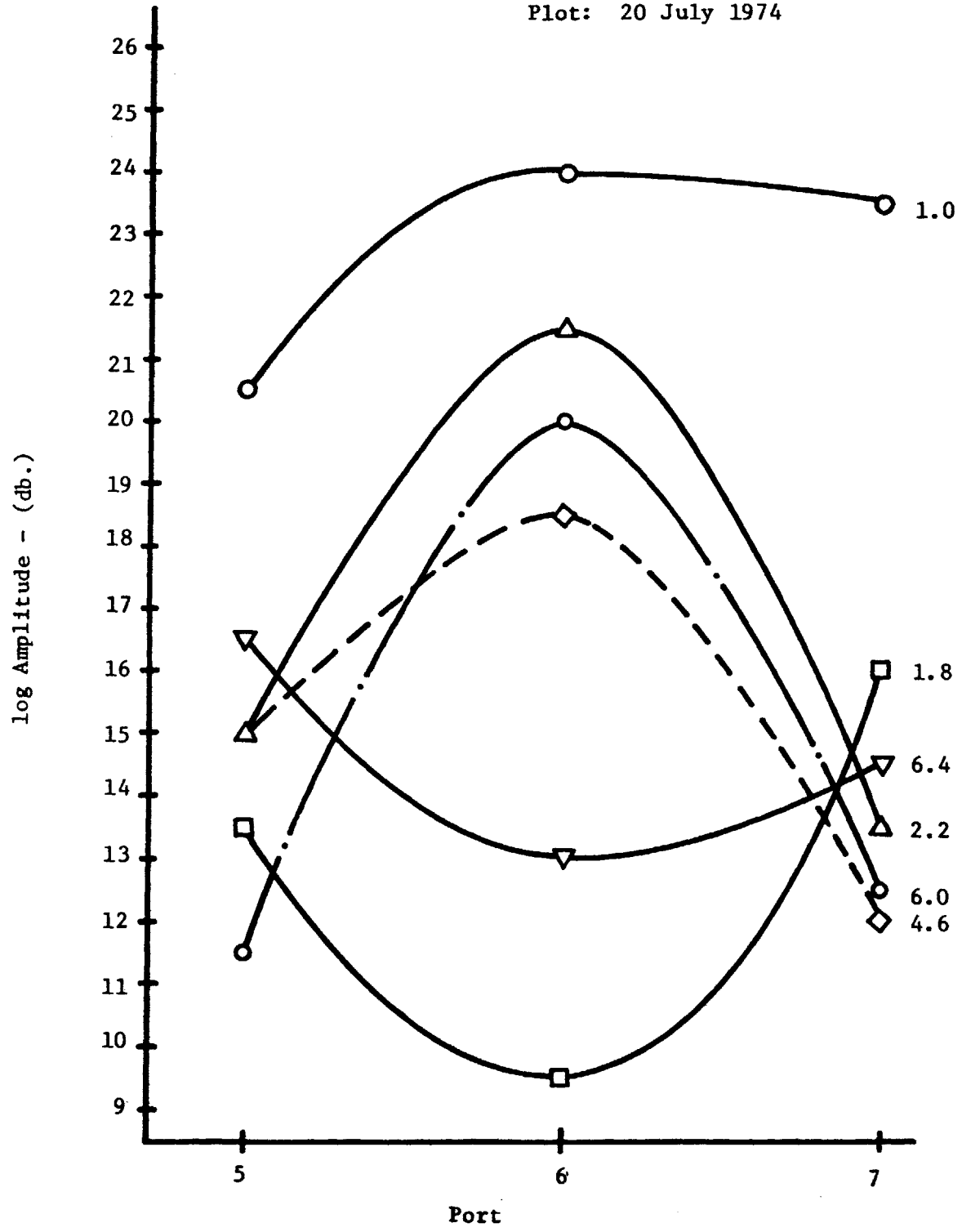
Wall Static Pressure
Frequency Dominant at Port 7
Data: 12, 13 July 1974
Plot: 20 July 1974
log Amplitude - (db.)
26
25
24
23
22
21
20
19
18
17
16
15
14
13
12
11
10
9
5
6
7
Port
1.0
1.8
6.4
2.2
6.0
4.6

Figure 24

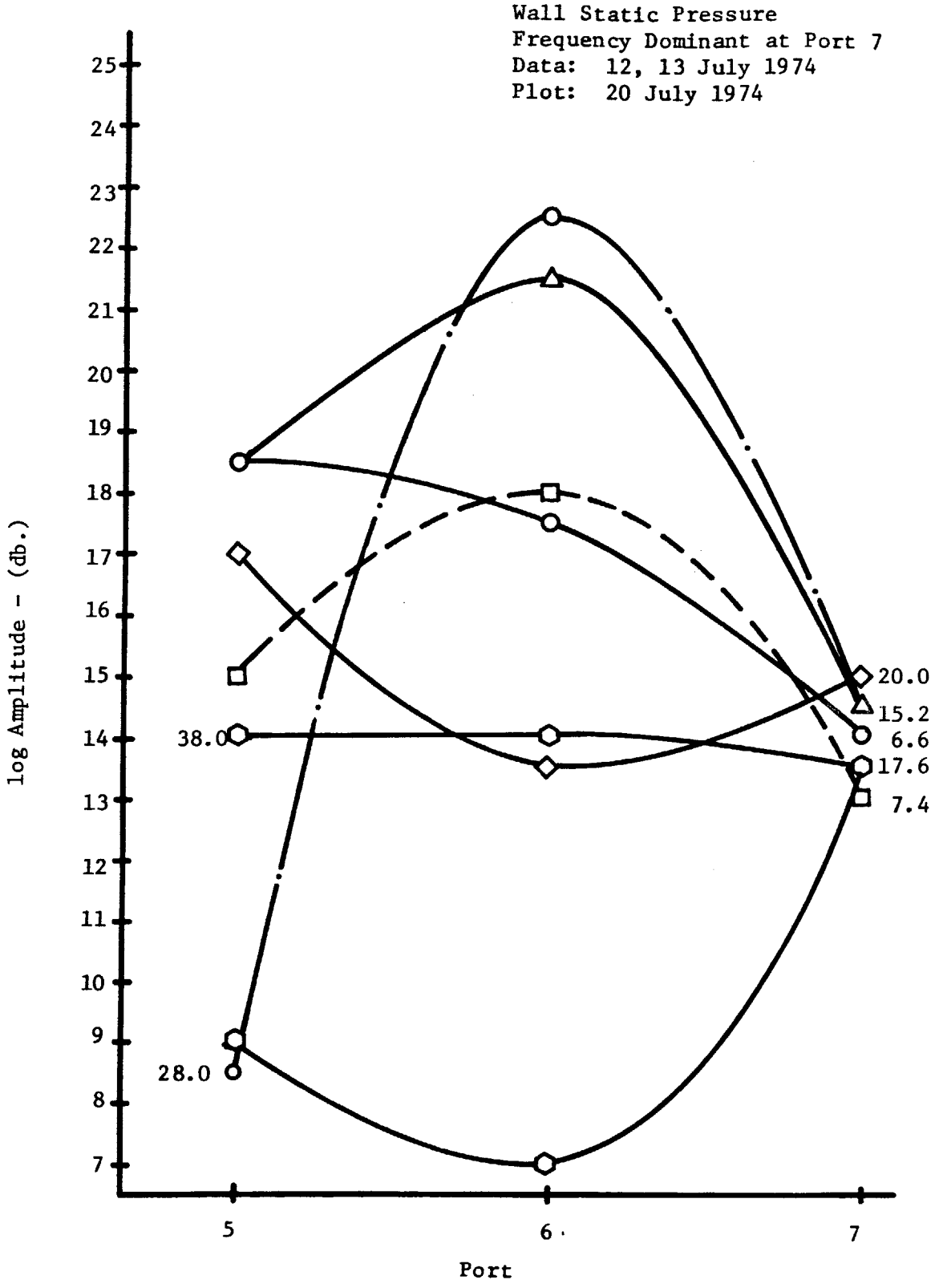
Wall Static Pressure
Frequency Dominant at Port 7
Data: 12, 13 July 1974
Plot: 20 July 1974
log Amplitude - (db.)
25
24
23
22
21
20
19
18
17
16
15
14
13
12
11
10
9
8
7
38.0
28.0
20.0
15.2
6.6
17.6
7.4
5
6
7
Port

Figure 25

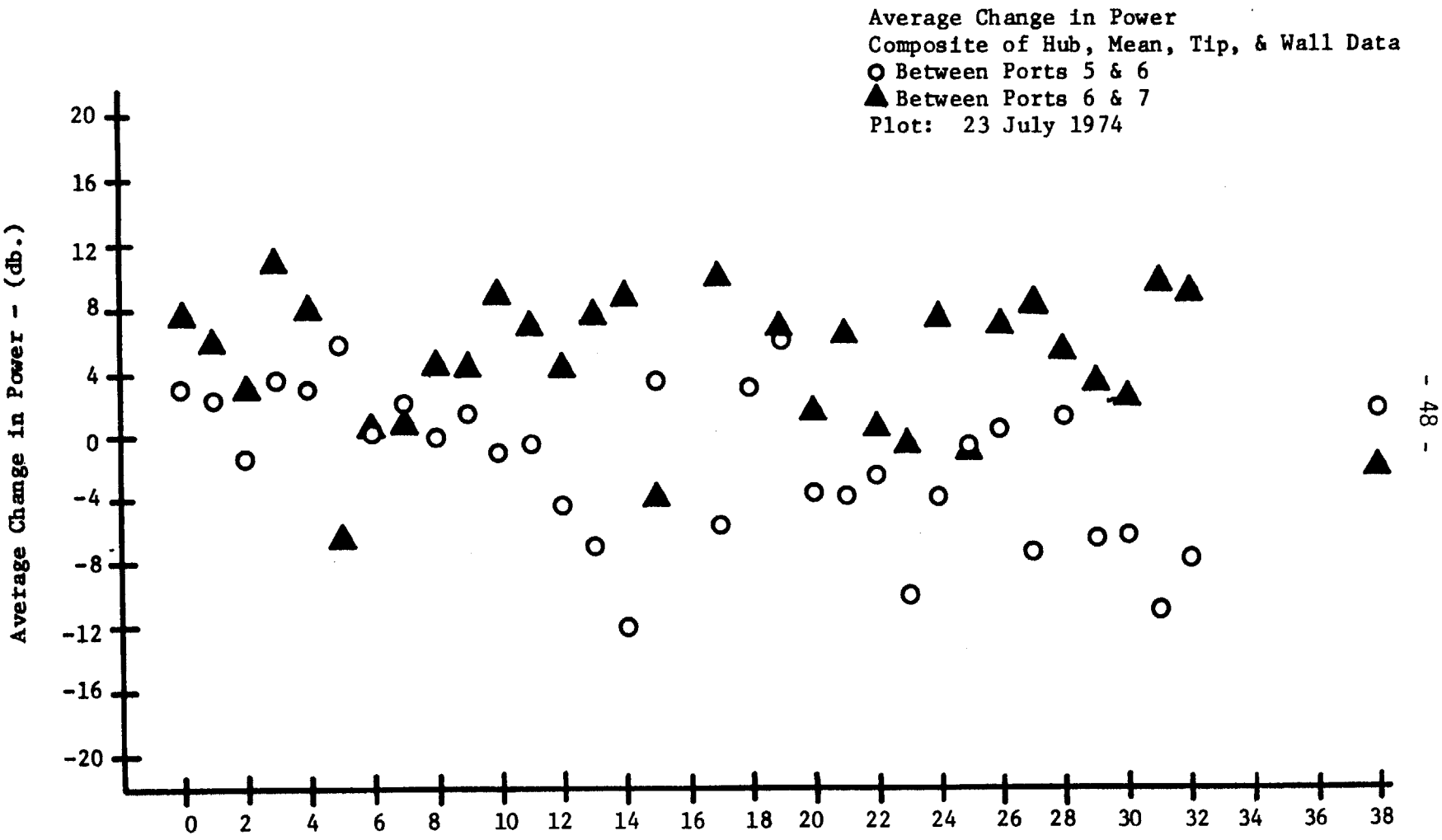
Average Change in Power
Composite of Hub, Mean, Tip, & Wall Data
Between Ports 5 & 6
Between Ports 6 & 7
Plot: 23 July 1974
Average Change in Power - (db.)
20
16
12
8
4
0
-4
-8
-12
-16
-20
0 2 4 6 8 10 12 14 16 18 20 22 24 26 28 30 32 34 36 38
Frequency Ratio

Figure 26

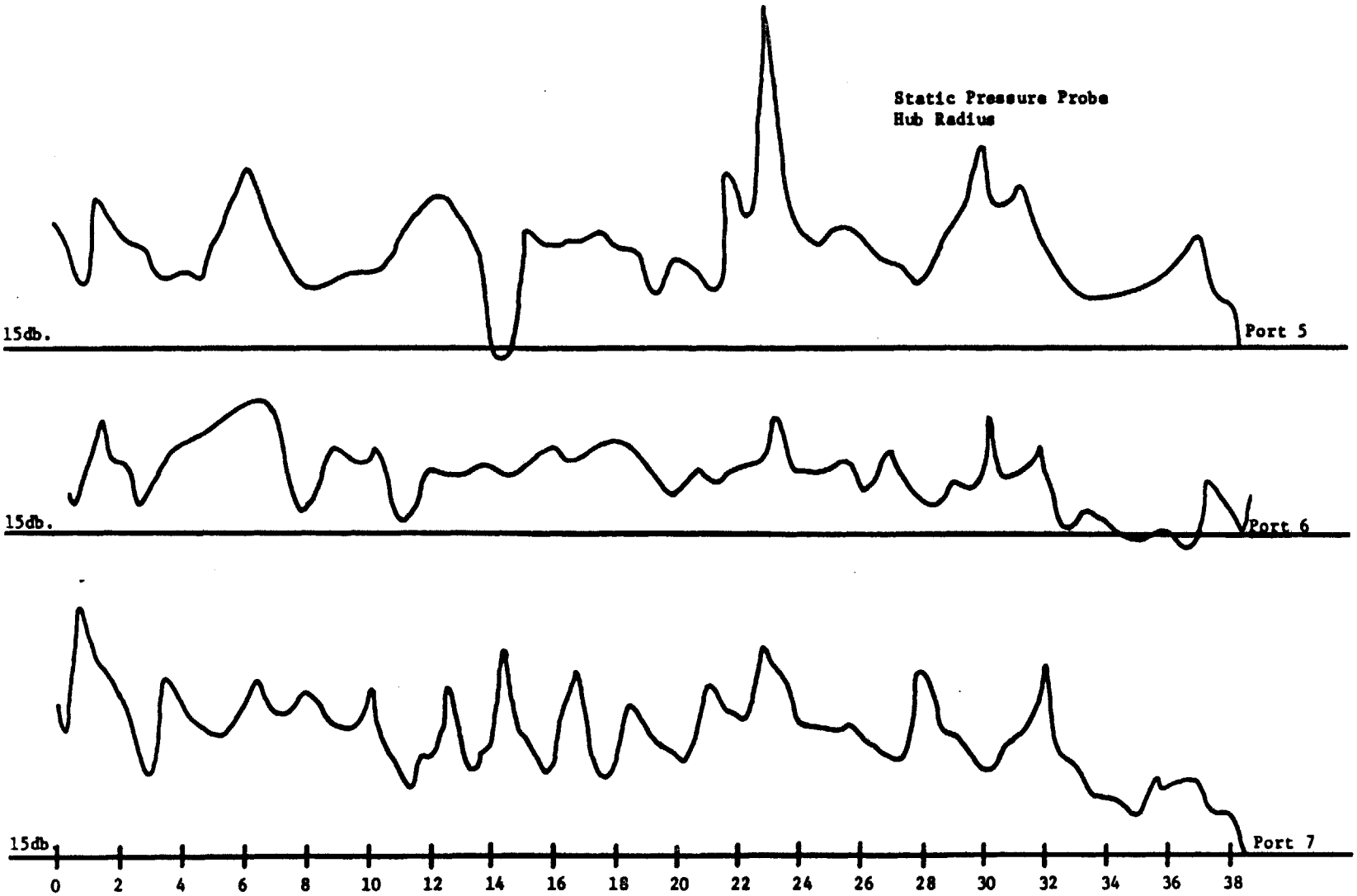


Frequency Ratio

Figure 27

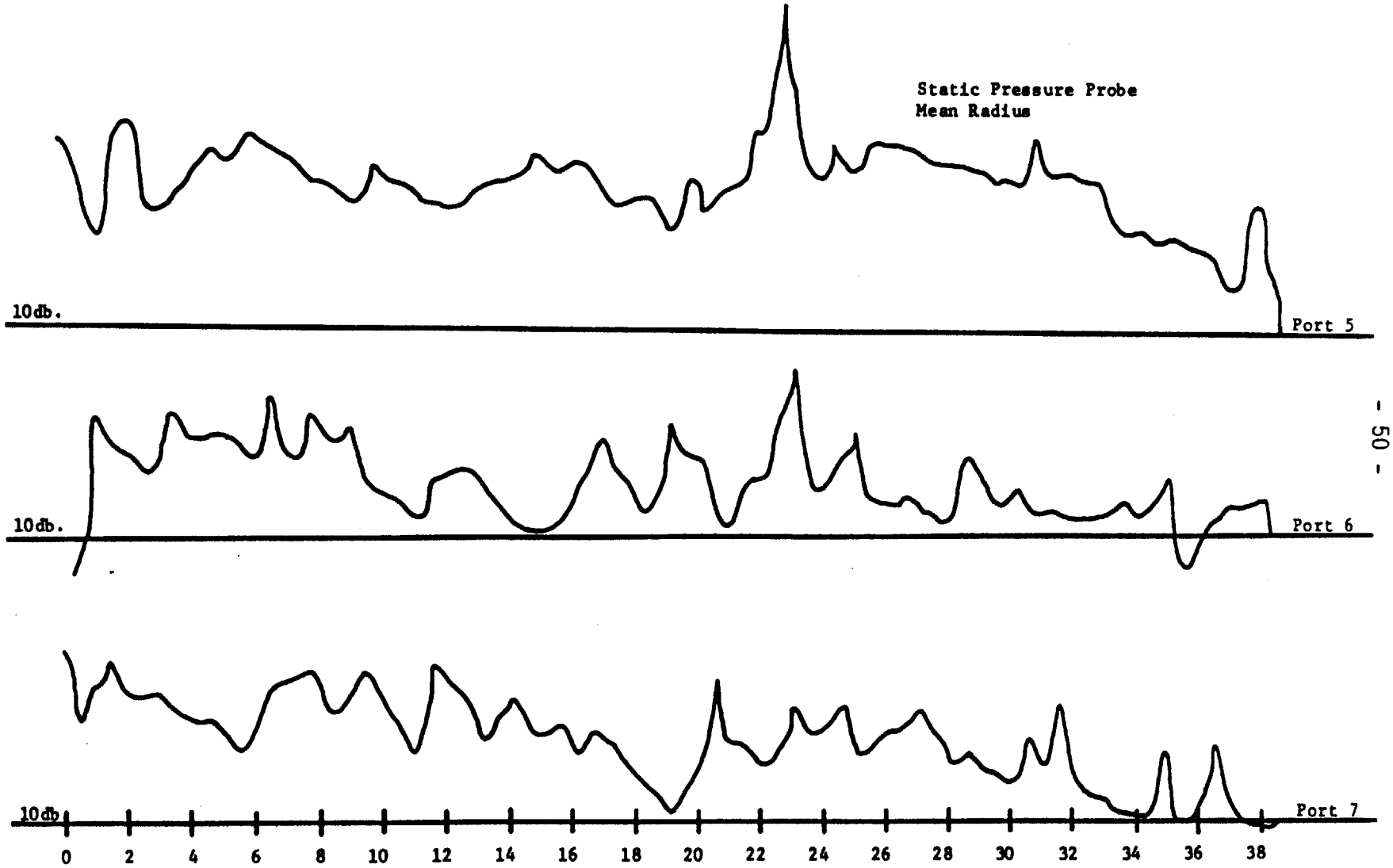


Frequency Ratio

Figure 28

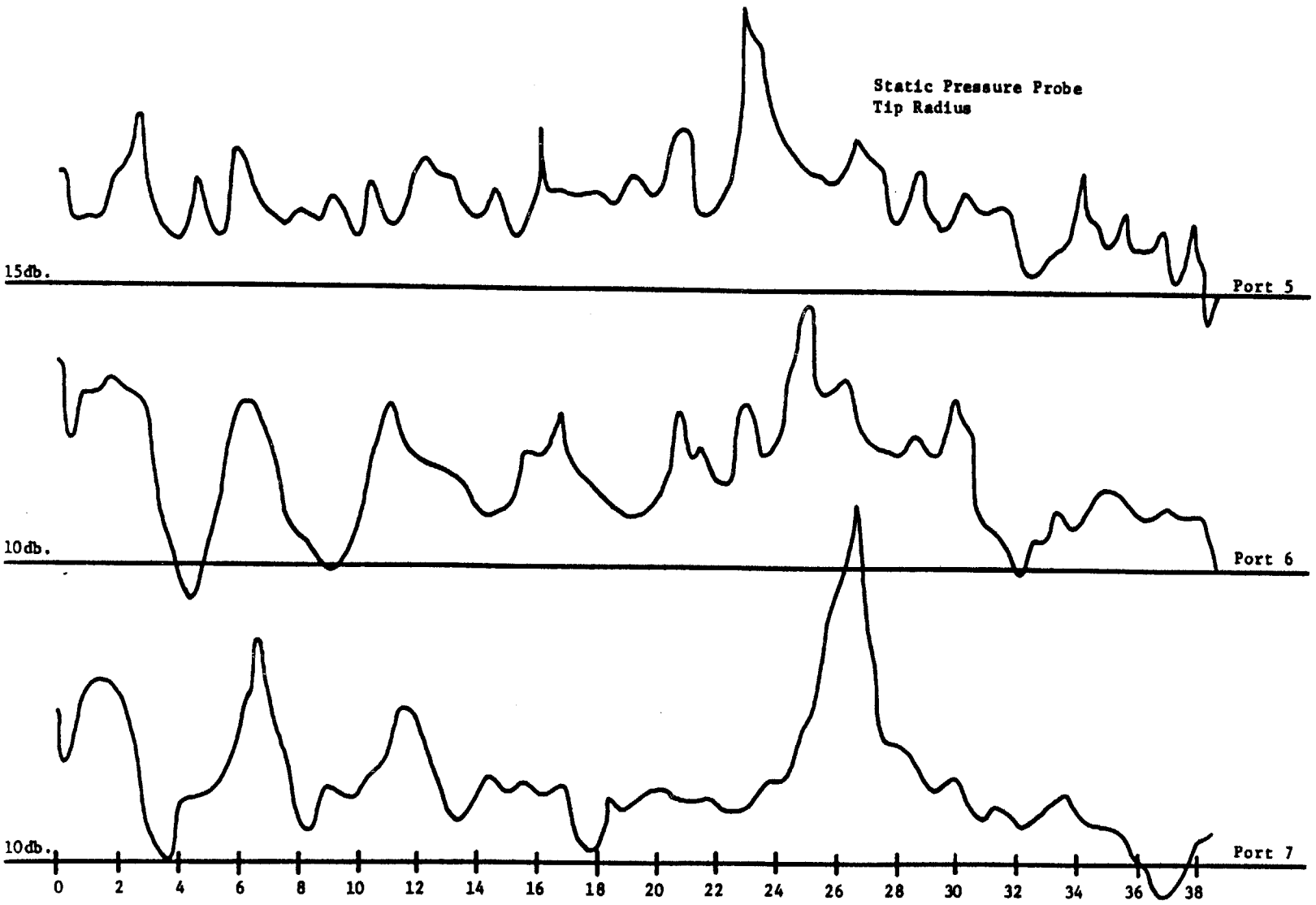


Frequency Ratio

Figure 29

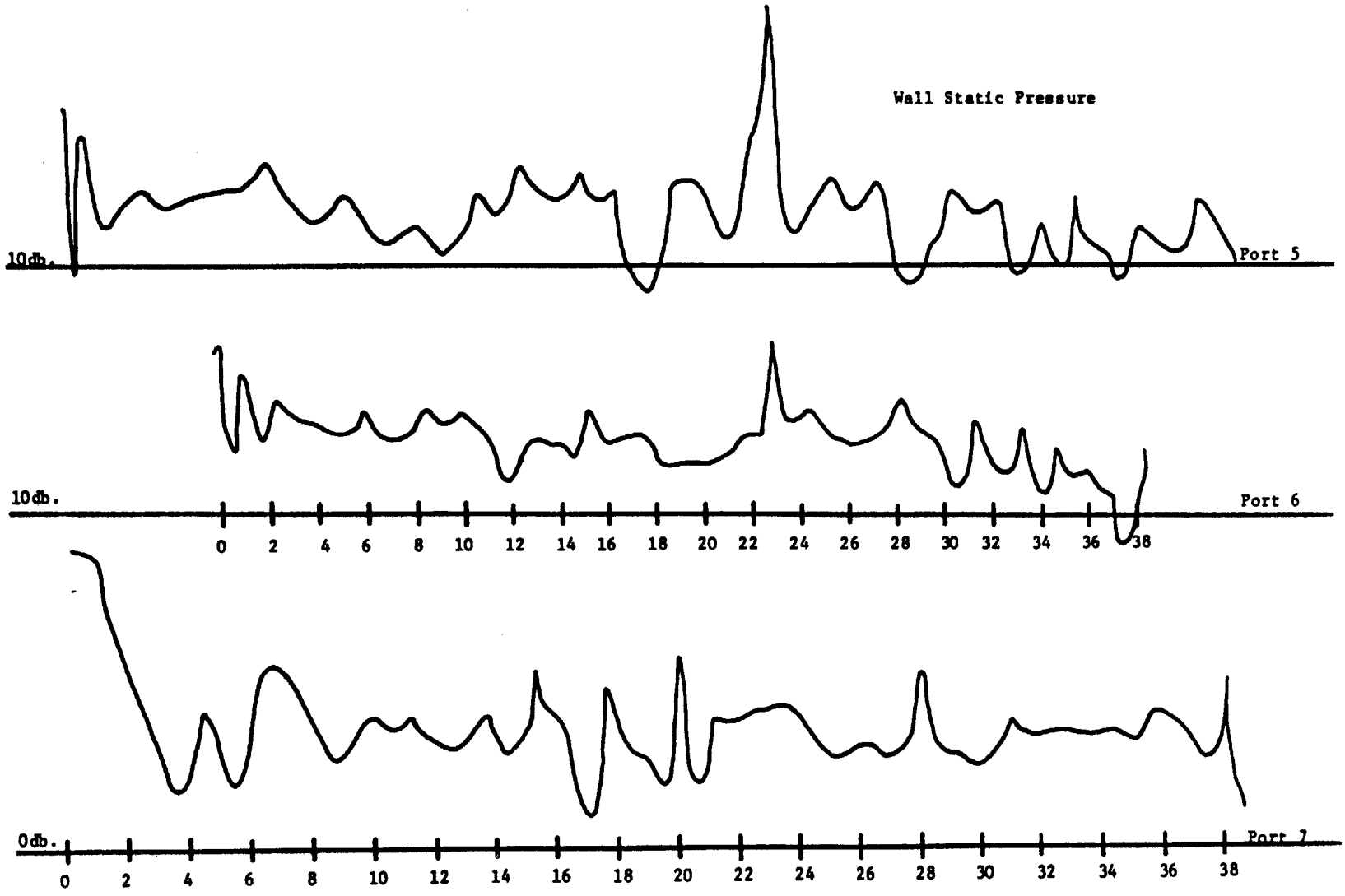


Frequency Ratio

Figure 30

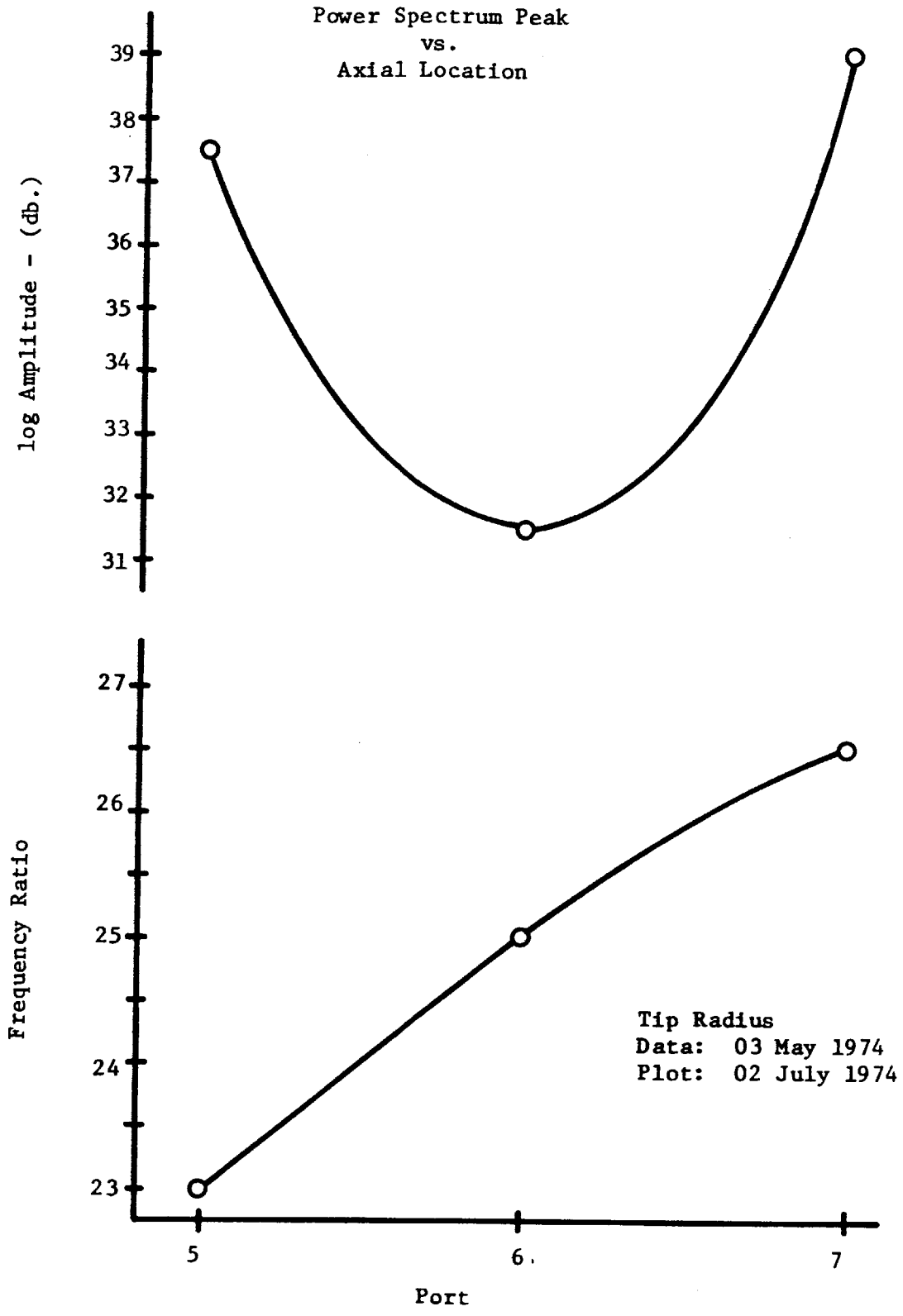
Power Spectrum Peak
vs.
Axial Location
log Amplitude - (db.)
39
38
37
36
35
34
33
32
31
Frequency Ratio
27
26
25
24
23
5
6
7
Port
Tip Radius
Data: 03 May 1974
Plot: 02 July 1974

Figure 31

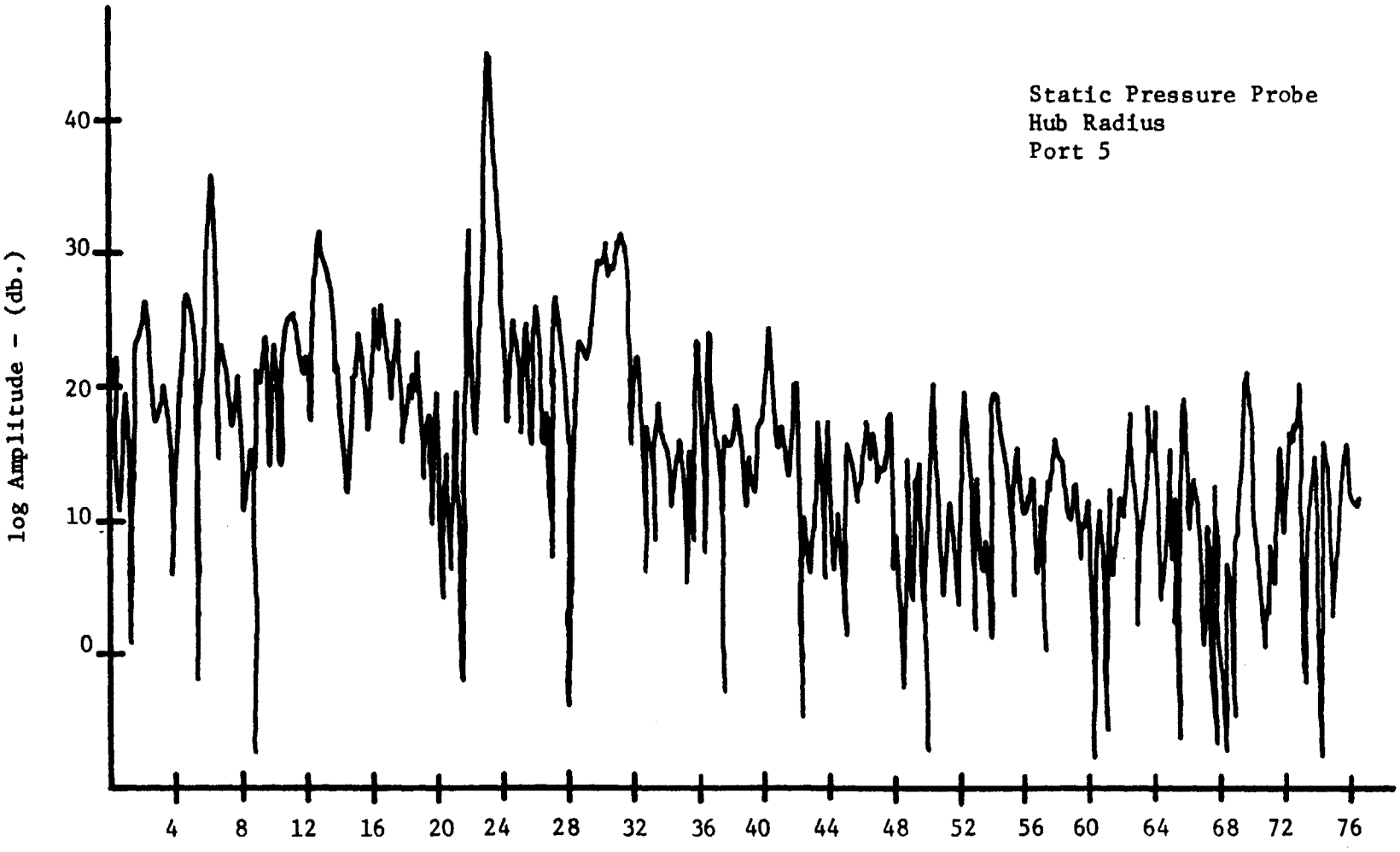
Static Pressure Probe
Hub Radius
Port 5
log Amplitude - (db.)
40
30
20
10
0
4
8
12
16
20
24
28
32
36
40
44
48
52
56
60
64
68
72
76
Frequency Ratio

Figure 32

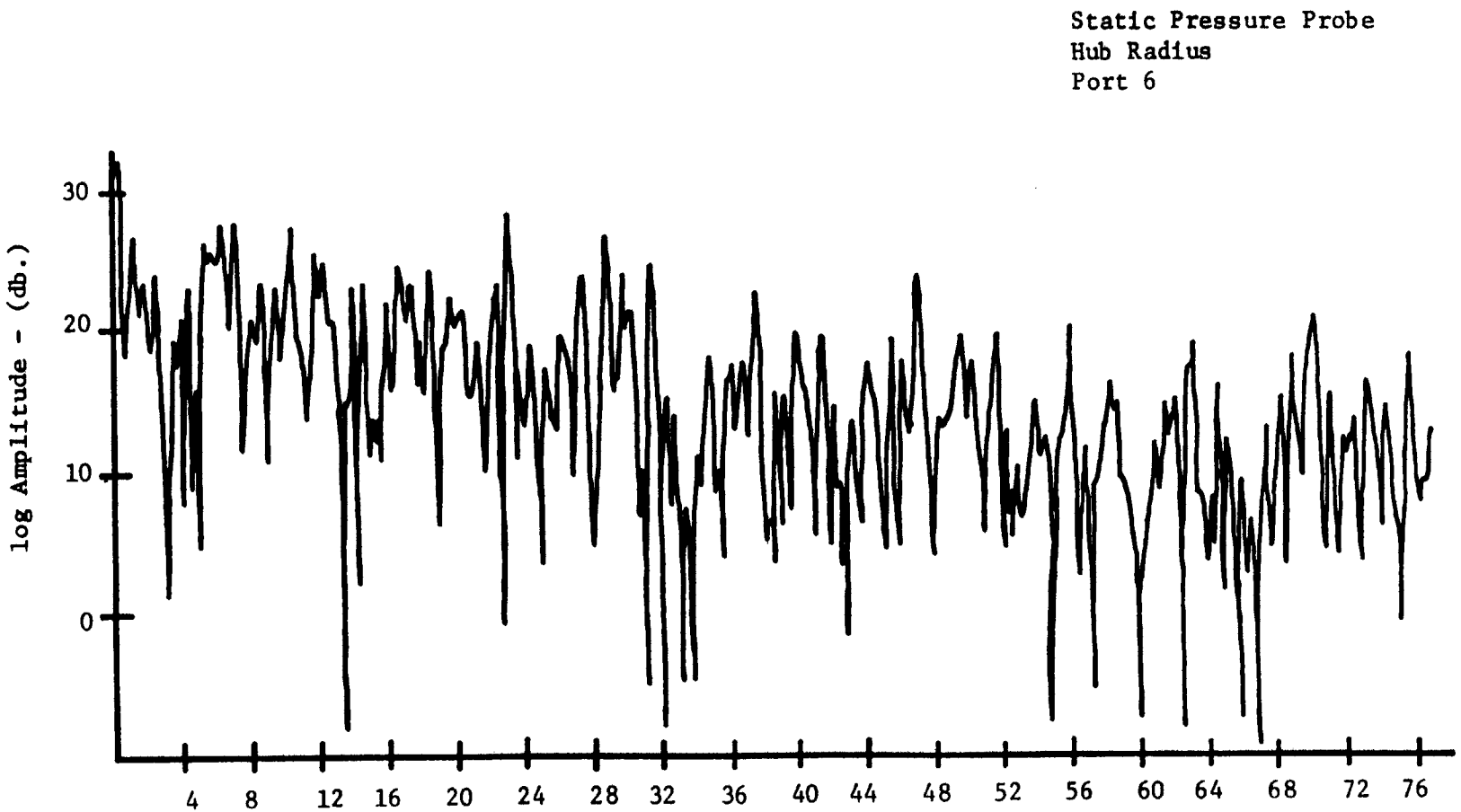
Static Pressure Probe
Hub Radius
Port 6
log Amplitude - (db.)
30
20
10
0
4
8
12
16
20
24
28
32
36
40
44
48
52
56
60
64
68
72
76
Frequency Ratio

Figure 33

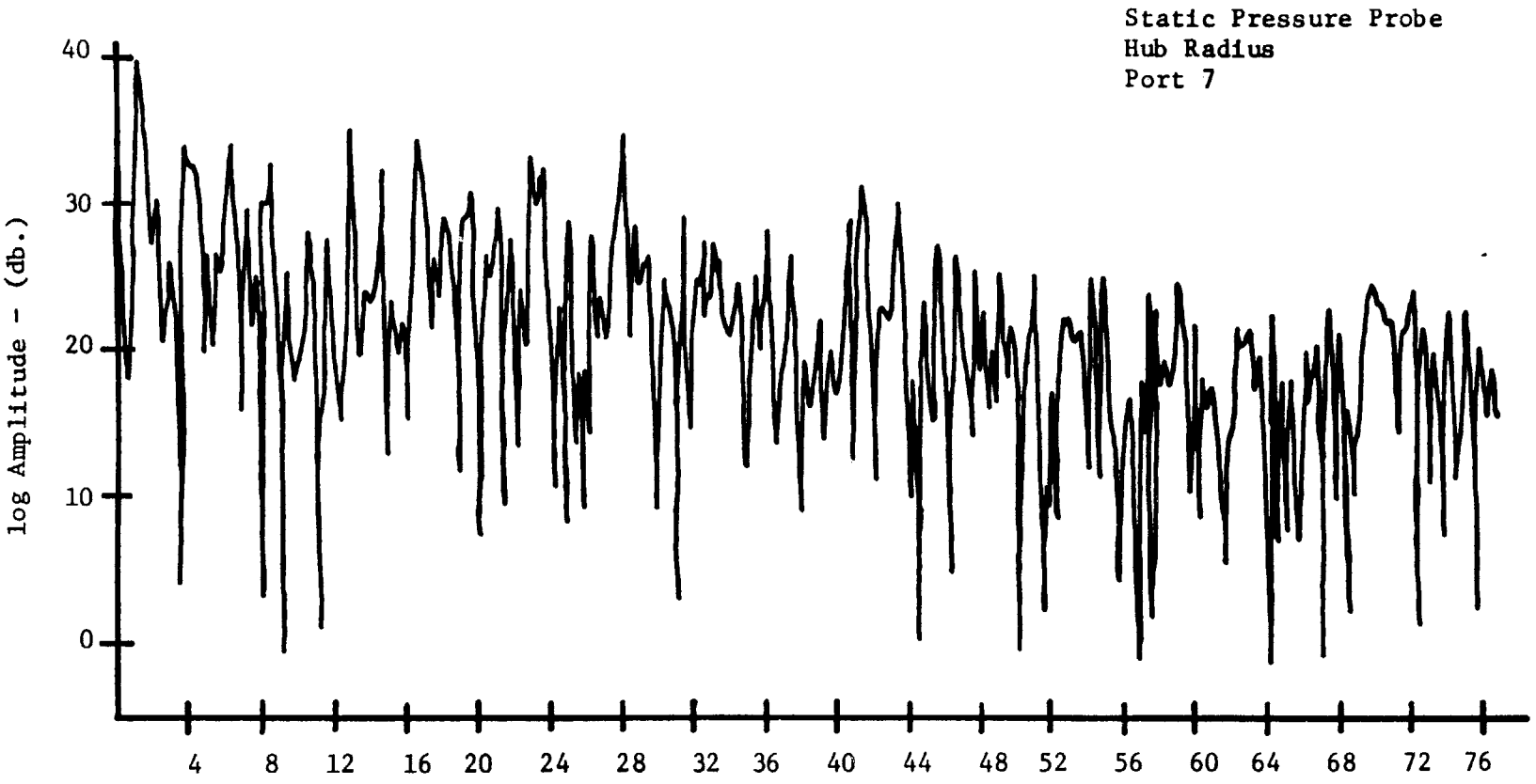
Static Pressure Probe
Hub Radius
Port 7
log Amplitude - (db.)
40
30
20
10
0
4
8
12
16
20
24
28
32
36
40
44
48
52
56
60
64
68
72
76
Frequency Ratio

Figure 34

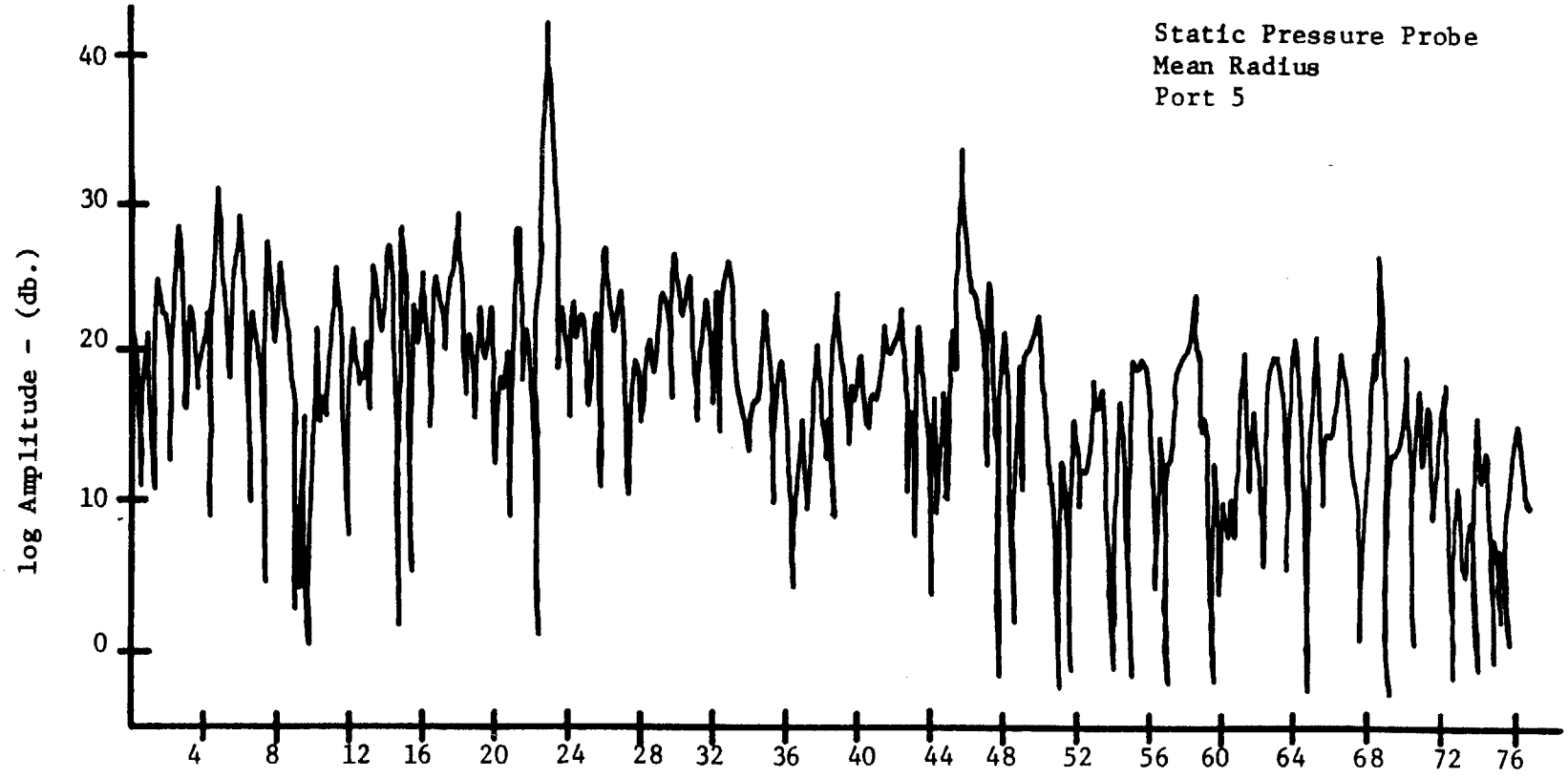
Static Pressure Probe
Mean Radius
Port 5
log Amplitude - (db.)
40
30
20
10
0
4
8
12
16
20
24
28
32
36
40
44
48
52
56
60
64
68
72
76
Frequency Ratio

Figure 35

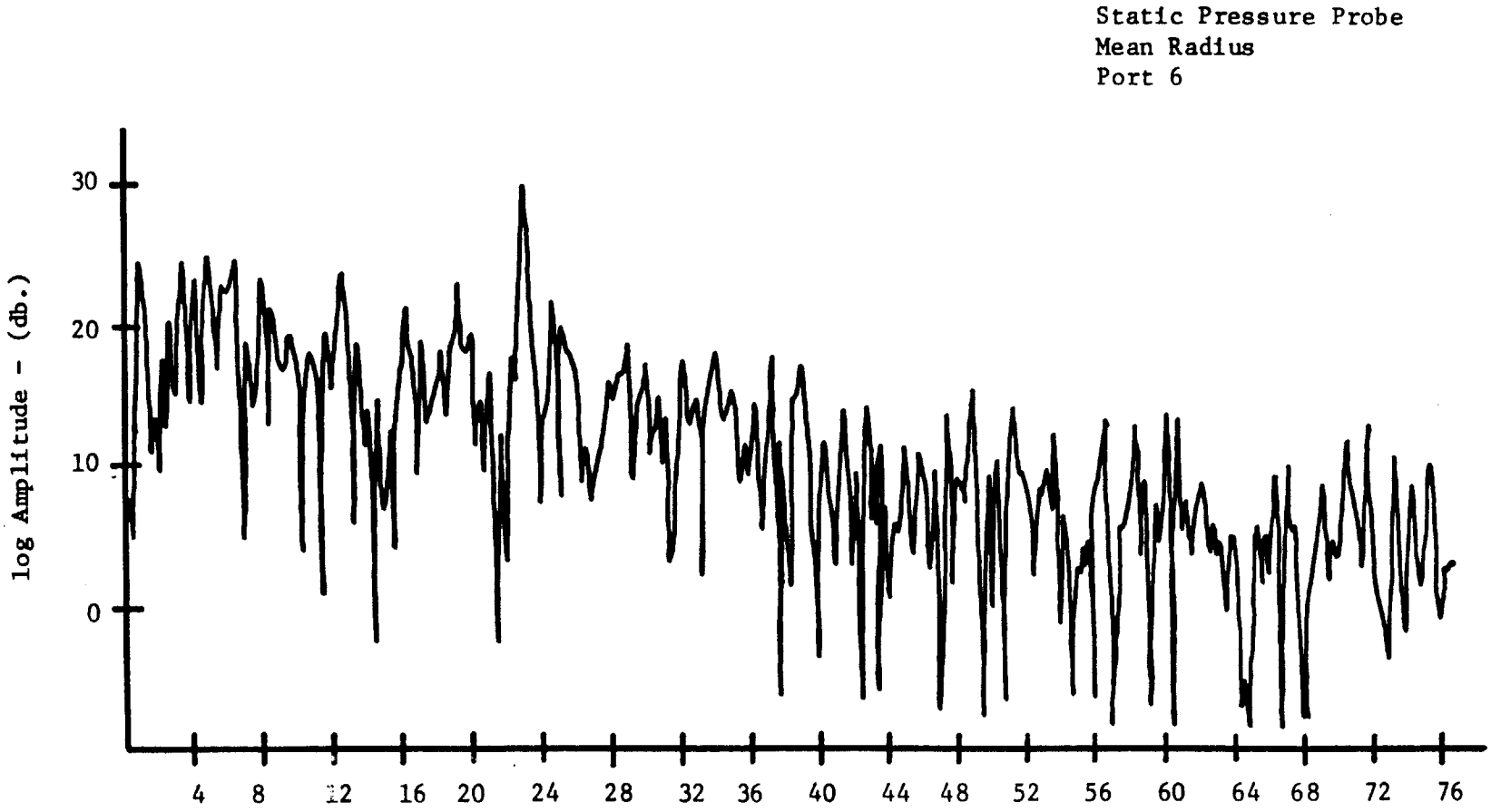
Static Pressure Probe
Mean Radius
Port 6
log Amplitude - (db.)
30
20
10
0
4
8
12
16
20
24
28
32
36
40
44
48
52
56
60
64
68
72
76
Frequency Ratio

Figure 36

Static Pressure Probe
Mean Radius
Port 7

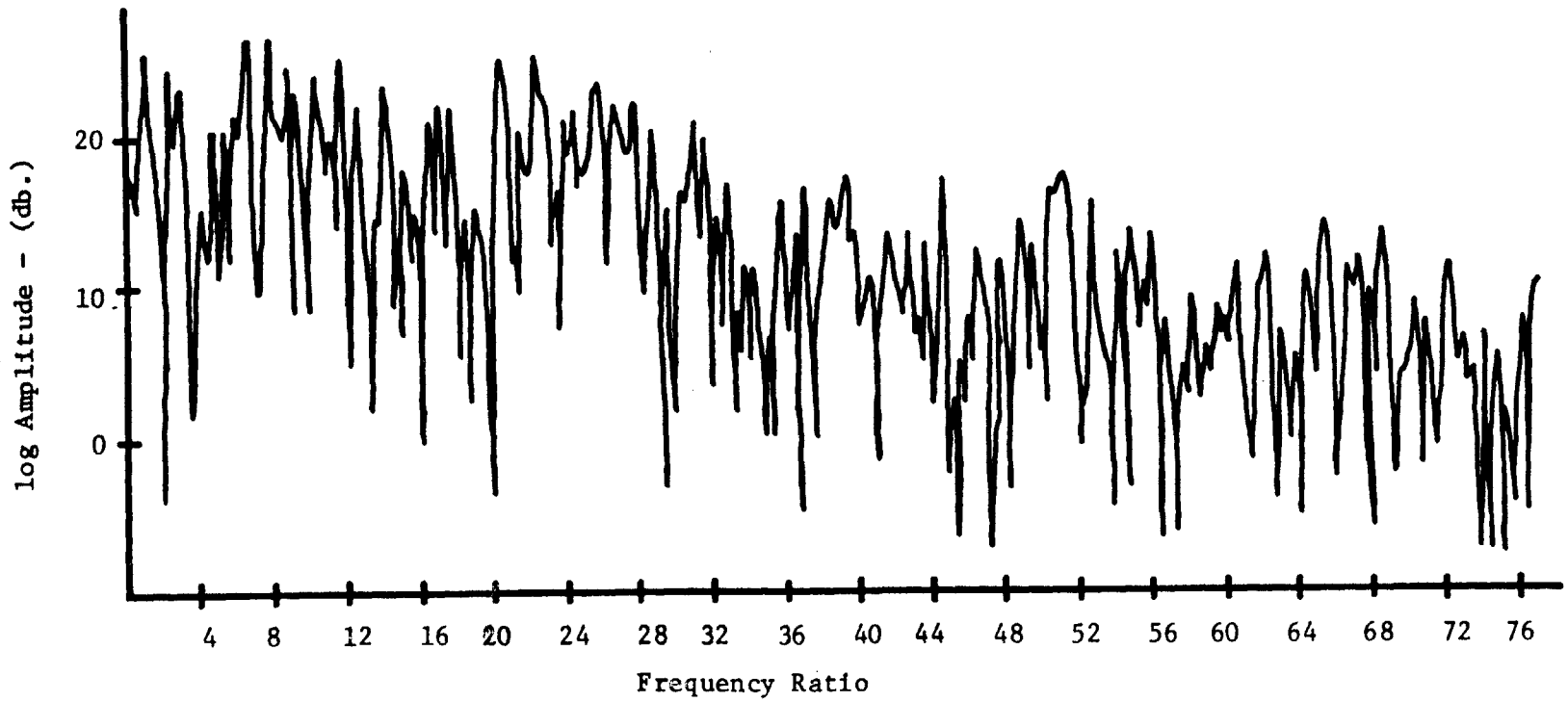


Figure 37

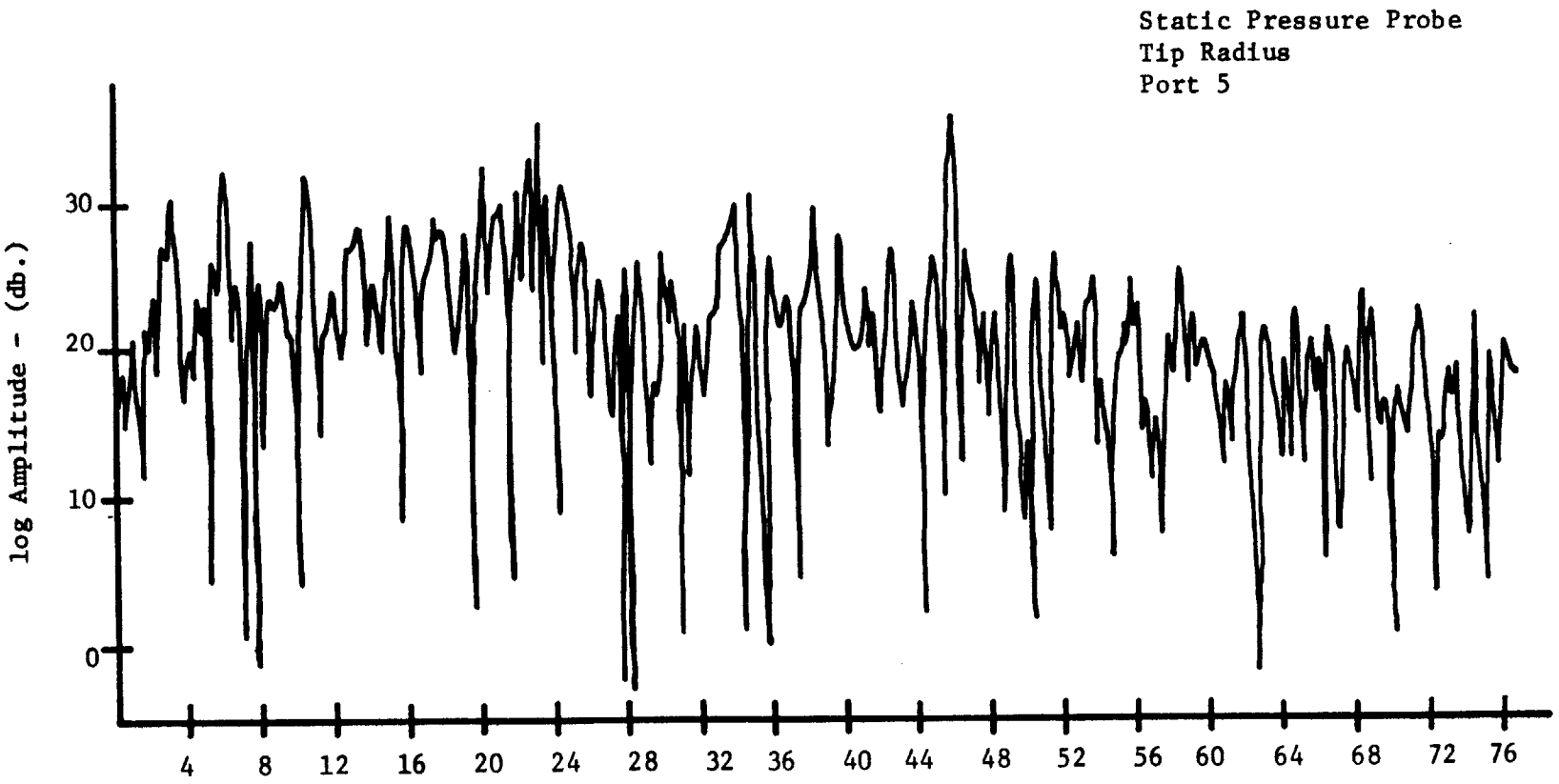
Static Pressure Probe
Tip Radius
Port 5
log Amplitude - (db.)
30
20
10
0
4
8
12
16
20
24
28
32
36
40
44
48
52
56
60
64
68
72
76
Frequency Ratio

Figure 38

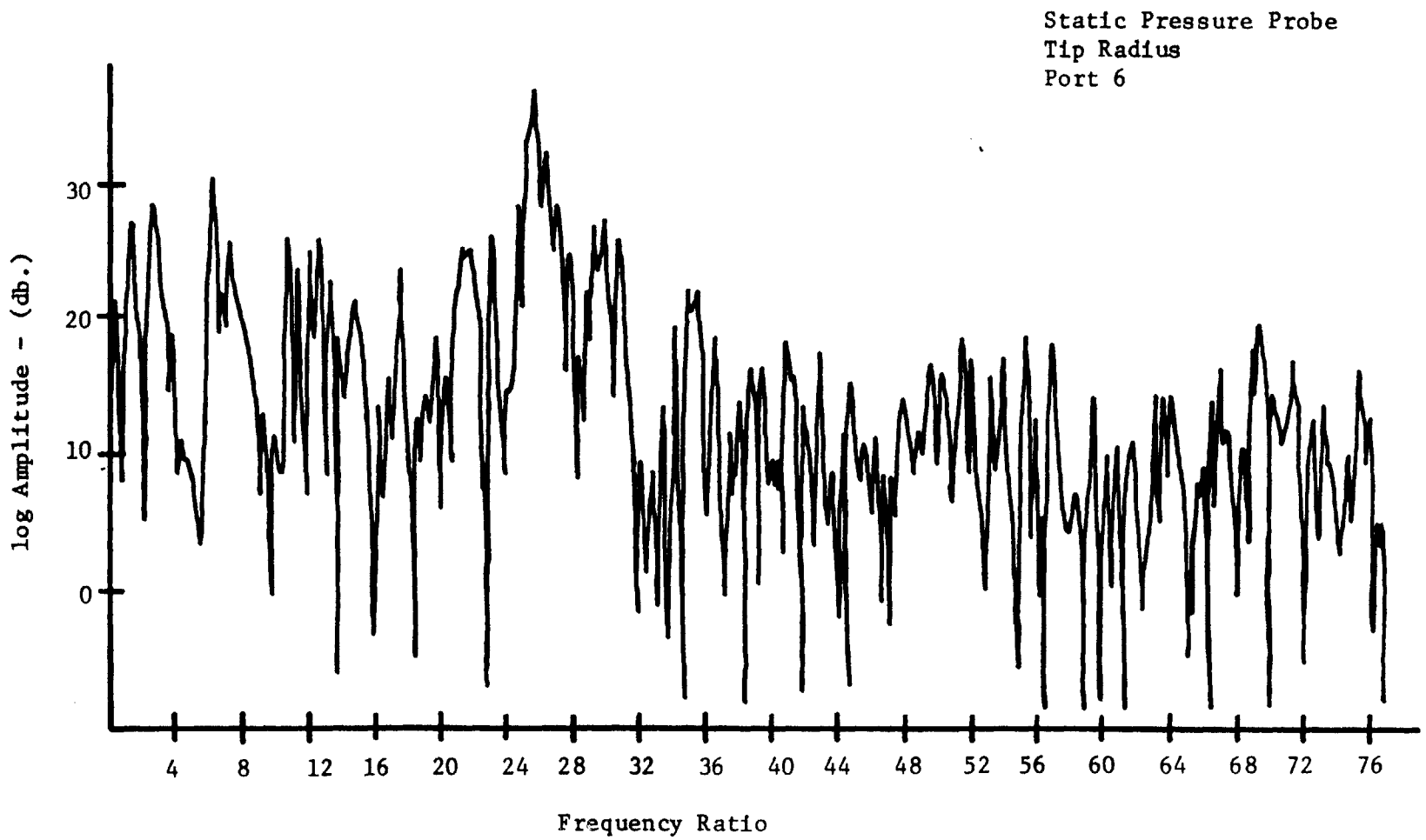
Static Pressure Probe
Tip Radius
Port 6
log Amplitude - (db.)
30
20
10
0
4
8
12
16
20
24
28
32
36
40
44
48
52
56
60
64
68
72
76
Frequency Ratio

Figure 39

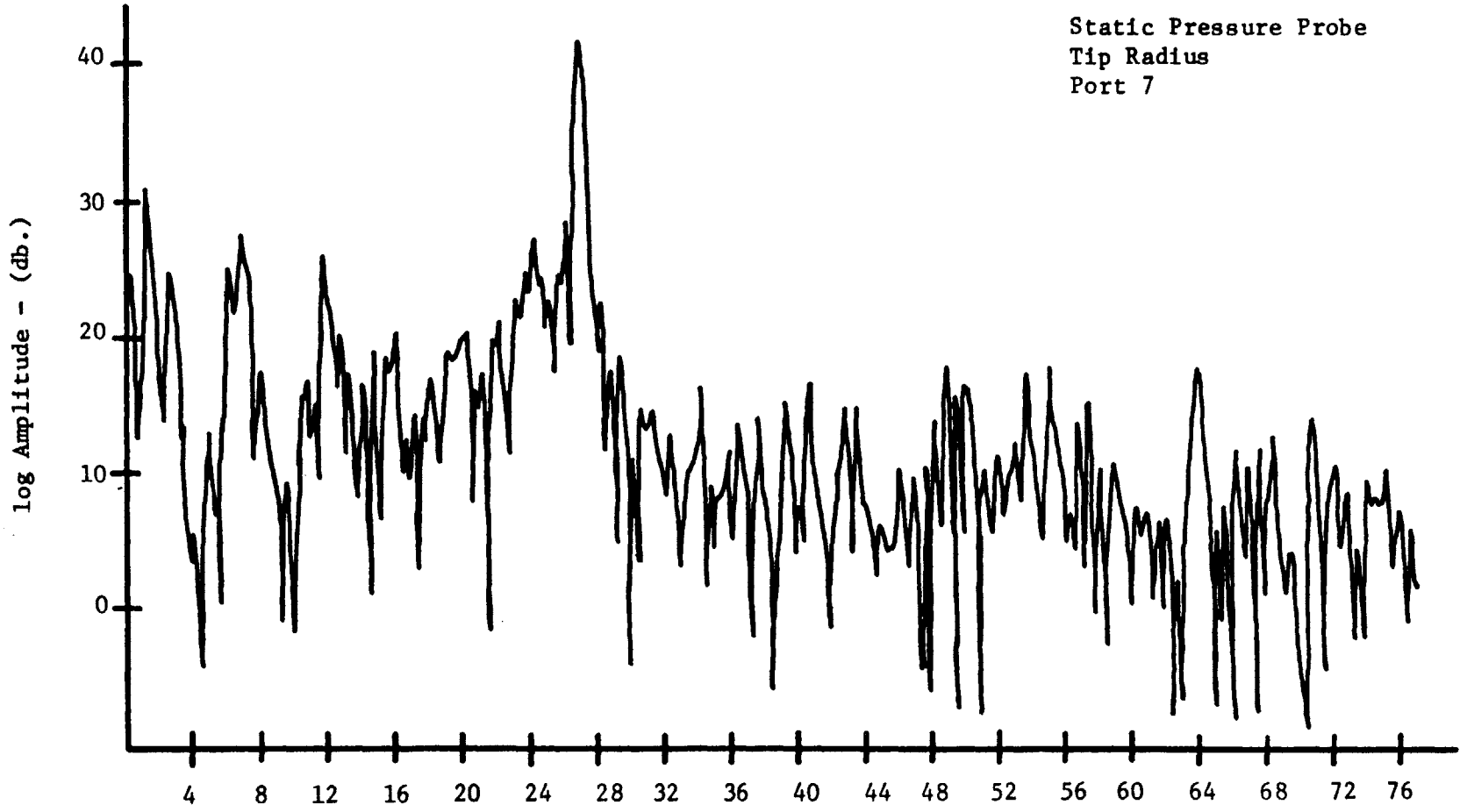
Static Pressure Probe
Tip Radius
Port 7
log Amplitude - (db.)
40
30
20
10
0
4
8
12
16
20
24
28
32
36
40
44
48
52
56
60
64
68
72
76
Frequency Ratio

Figure 40

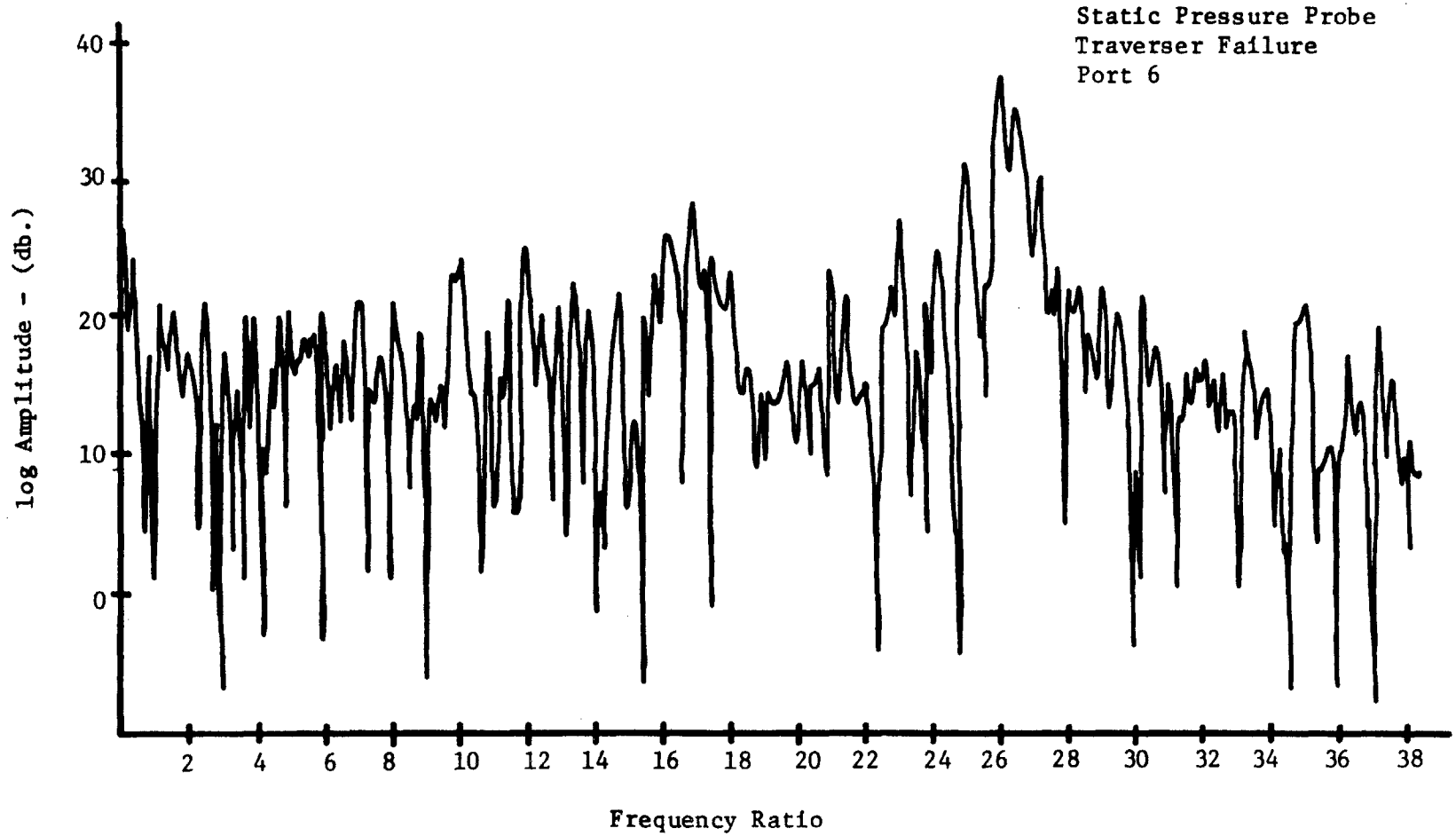
Static Pressure Probe
Traverser Failure
Port 6
log Amplitude - (db.)
40
30
20
10
0
2
4
6
8
10
12
14
16
18
20
22
24
26
28
30
32
34
36
38
Frequency Ratio

Figure 41

## REFERENCES

1. Evans, R. L., "Turbulence and Unsteadiness Measurements Downstream of a Moving Blade Row," ASME Paper No. 74-GT-73 (1974).

2. Haines, D. M., "Wake Behavior Behind a Transonic Rotor," S.M. Thesis, Massachusetts Institute of Technology, Sept. 1973.

3. Kerrebrock, J. L., "The M.I.T. Blowdown Compressor Facility," M.I.T. Gas Turbine Lab. Report No. 108, May 1972.

4. Kerrebrock, J. L., "The M.I.T. Blowdown Compressor Facility," ASME Paper No. 74-GT-47 (1974).

5. Kerrebrock, J. L., "Waves and Wakes in Turbomachine Annuli with Swirl," AIAA Paper No. 74-87 (1974).